Vehicle Positioning with Magnets in a Carriageway

Jonas Steverud
Matts-Ola Wessman
Fabio Santandrea

ÅF AB

Abstract

Positioning a vehicle on the carriageway is a crucial function for a vast number of applications within automotive safety and autonomous drive. This report describes a study performed to propose a working system for the Swedish road network. A prototype was designed and tested at speeds up to 165 km/h and a model-based signal processing algorithm was designed to position the vehicle in a global coordinate system. The magnetic field intensity from neodymium and ferrite magnets where studied and a proposal is made for an appropriate magnet and pattern of magnetic markers. The conclusion is that a full scale system is possible to achieve within the constraints set by the project's parameters.

Table of contents

1 Background

The possibility to accurately measure the position of a vehicle on the public road network is crucial to a number of different situations, which includes but are not limited to lane positioning when the vehicle is driving on a multi-lane carriageway, guidance and information of exact position to the driver e.g. for road maintenance vehicles and guidance and navigation for autonomous vehicles.

One method that has been investigated by several research bodies is to bury permanent magnets below the road surface. The California PATH [1] project is probably one of the more well-known studies. The vehicle has a row of sensors that detects the magnets and the system calculates the position of the vehicle relative to the magnets and hence the position of the vehicle relative to the road.

The Swedish Transportation Administration has initiated a study to investigate the feasibility of such a system for the Swedish road network. Volvo Car Corporation and ÅF have partnered to investigate the technological issues as well as the feasibility to use such a system on the Swedish public road network. The result is included in this report.

2 Project definition

The purpose of this research project is to investigate if it is feasible to use permanent magnets for positioning of vehicles on the Swedish public road network. A sensor prototype should be designed and implemented and the total system (sensor and magnetic markers) should be analysed.

In this section a summary of the major research questions and system requirements that defines the project are presented.

2.1 Environment and availability

- The system should be free of extra maintenance relative to the lifetime of comparable vehicle components and the carriageway.
- The system should work in predictable environments e.g. in regards to snow, ice and electrical disturbances.
- The system should be active in speeds up to 150 km/h (42 m/s) and as long as any set of wheels are on the carriageway.

2.2 Positioning capability

- Lateral positioning error should be less than 0.1 m after a maximum distance of 10 m into the magnetic pattern.
- Longitudinal positioning error should be less than 1.0 m after a maximum distance of 50 m into the magnetic pattern.
- The system should be able to detect any errors in the magnetic marker pattern caused by accident or tampering.

2.3 System design

The components and sub-systems of the prototype system design should meet the cost requirements of a large scale realization. If other more expensive components are used, the performance or results should be compensated, to match the cost requirements.

2.3.1 Sensor system capability

Analyse the following parameters considering positioning capability and cost.

- Type and number of magnetic sensors in the system
- Sensor integration in the vehicle

Propose an algorithm for positioning of the vehicle using information from the magnetic sensor fused with GPS and inertial navigation signals.

2.3.2 Magnetic pattern

- Analyse what type of magnets is suitable for this application. Is there an optimal size?
- Find a pattern of magnetic markers that fulfils the positioning and cost requirements.
- Investigate the trade-off between sensor and infrastructure cost.
- Information can be coded into the pattern of magnetic markers. Investigate what kind of information is suitable to code using magnets and what information should be available in a cloud based vehicle system.

2.3.3 Estimated cost

- The cost of the system should be less than 500 SEK/unit at a sales volume of 50,000 units per year.

3 Theoretical Framework

3.1 Some definitions

For the rest of the report, the magnet is defined by the parameters shown in Figure 1 below. A cylindrical magnet is always assumed and no other form is used unless otherwise stated, see also section 9.

The coordinate system The coordinate system is defined as a right hand system with the z along the major axis of the cylinder and origin at the centre of the magnet. The magnet has the magnetisation along the z-axis.

l_m The length of the magnet.

d_m The diameter of the magnet.

h_s The height at which the sensor is located, or the height the magnetic field intensity is measured.

h The height at which the magnetic field intensity is measured, usually the same as h_s.

Throughout this report the origin of the magnet is in the centre of the magnet and the height of the sensor is the z-coordinate of the sensor. Sometimes it is more convenient to discuss the distance from some object along the z-axis and the top of the magnet, this is usually the case when the marker inserted in the carriageway is discussed. It will be explicitly stated if another origin than the centre of the magnet is used during a discussion.

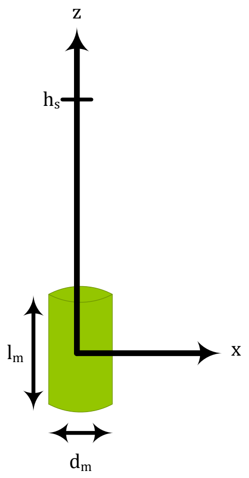

Figure 1 The parameters defining a magnetic marker.

3.2 Magnetic field theory

The dipole model for a magnet sees the magnetic poles as points in space slightly distanced from each other. A cylindrical magnet can be modelled according to this model with high accuracy at a sufficiently large distance. Only cylindrical magnets are considered in this report as other geometries as rings and cuboids all have weaker magnetic fields, see also section 6.2.1. The dipole model provides an adequate description of the field generated by an arbitrarily shaped magnetic source as long as the distance between the magnetic source points are much smaller than the distance between the points and the sensor.

A more accurate model to describe the magnet is the analytical cylinder model, described in [2]. The dipole model was used for analysis and development but the cylindrical model was used for all simulations of the magnetic field in this report. The difference between the two models is shown in Figure 2. The models differs significantly as long as the point is inside the magnet but when the measurement point until z=2.5 cm where the field leaves the magnet and after an additional few centimetres the difference is very low but high enough to be of some concern.

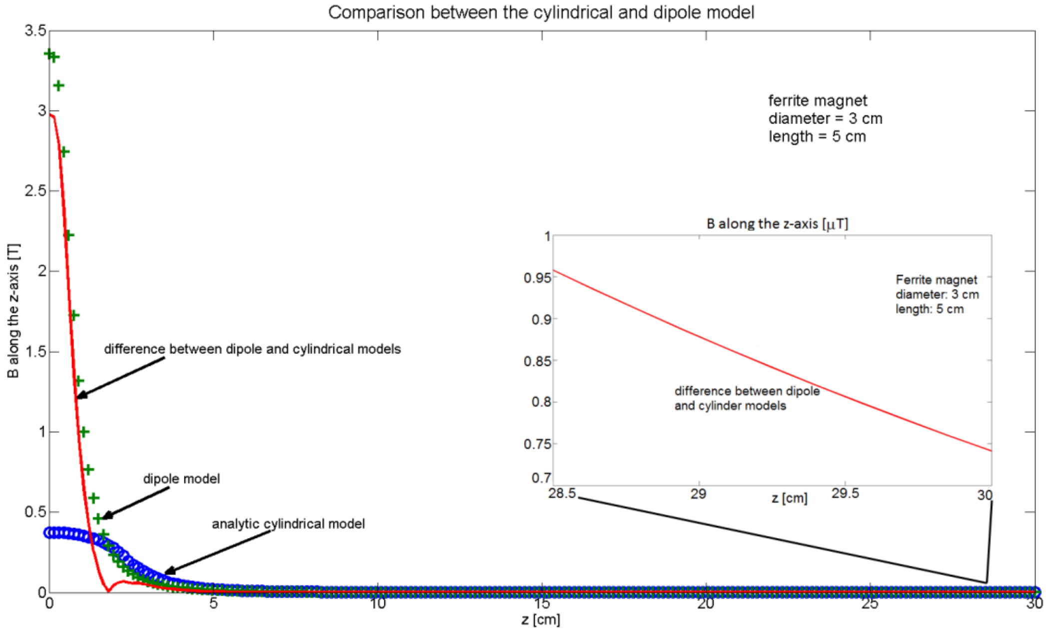

Figure 2 Comparison between the cylindrical and the dipole magnetic models

The difference between the two models for a 3×5 cm ferrite is less than 1 µT at a height of approximately 30 cm and in Figure 44 it can be seen that the cylindrical model gives a field intensity of approximately 74 µT. This gives an error of 1 %. This is well below other noise sources and the dipole model is used in this report without modification for easier calculations.

The functions describing the magnetic field intensity is show in Equation 2 to Equation 4, where *m* is the magnetic moment of the magnet and *r* is the distance between the magnet and the sensor. The constant μ_0 is the permeability of free space and the constant B_r is the remanence field. In some calculations the μ_0 is replaced by $\mu = \mu_r \mu_0$ where μ_r is the relative permeability of the material which the field passes through, see section 3.2.1.2.

$$r = \sqrt{(x^2 + y^2 + z^2)}$$

Equation 1 Definition of the r for the magnetic field equations

$$B_x = \frac{3mxz}{r^5}$$

Equation 2 Magnetic field intensity along *x*-axis

$$B_y = \frac{3myz}{r^5}$$

Equation 3 Magnetic field intensity along *y*-axis

$$B_z = \frac{m(3z^2 - r^2)}{r^5}$$

Equation 4 Magnetic field intensity along *z*-axis

$$m = \mu_0 B_r V = \mu_0 B_r \pi \left(\frac{d}{2}\right)^2 l$$

Equation 5 Magnetic moment *m* for magnet of volume *V*, *d* is the diameter and *l* is the length of the magnet

These equations above shows that the magnetic field at a certain height *z*, e.g. 50 cm, from the centre of the magnet, directly above the magnet (i.e. $y=x=0$ in Equation 1, i.e. r=z) is a constant times the volume of the magnet. The ratios between the length and the diameter of the magnet do not affect the intensity as long as the distance from the magnet is larger than the dimensions of the magnet; it is the total volume that determines the field. A rule of thumb is to take the largest dimension of the magnet and as long the distance is longer than this the field does not depend on the ratio.

3.2.1 Magnetic field study

As the equations of the magnetic field shows, the field is a continuous field that decreases with the cubic distance; the field is defined by Equation 2 to Equation 4. For this report only neodymium and ferrite magnets have been used, neodymium is about three times stronger than ferrite for the same volume but about ten times more expensive.

The field detected by the sensor depends on the distance between the magnet and the sensor and in the following sections a study of the impact of the dimension, material and distance is presented. The intensity of the field on a given height above the ground resembles a Gaussian bell curve centred on the magnet's axis; see Figure 5 for an example.

3.2.1.1 The magnetic field in free space

The first study concerns a cylindrical magnet in free space and the field intensity is plotted on various heights and with various dimensions of the magnet; this is to have a general understanding of the field. For these calculations the analytical cylinder model was used. All graphs are included in the appendix, section 11.1, but some are included in this section for easier reference.

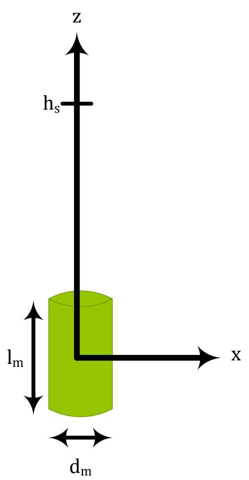

Figure 3 Parameter definition for parametric study in free space.

The parameters that will influence the detectable magnetic field are the physical dimensions of the magnet and the distance between the sensor and the magnet. A study was performed where the centre of the magnet was used as origin and the diameter, length and material of the magnet were varied and then the field was calculated along the x-axis for three sets of heights (30, 50 and 70 cm). The parameters are defined in Figure 3.

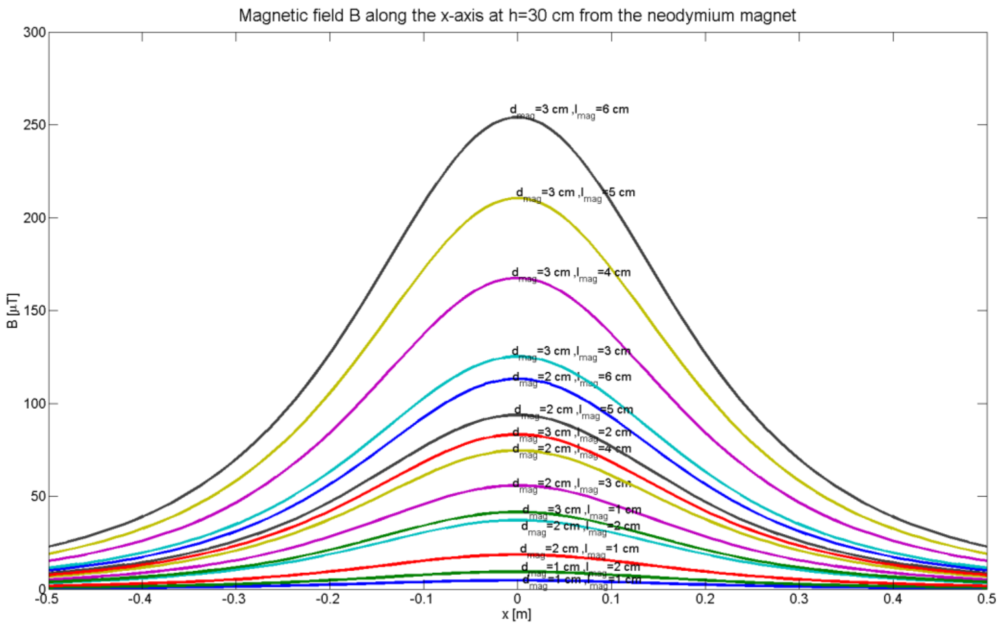

Figure 4 Magnetic field study, neodymium magnet at 30 cm height

What can be seen from Figure 4 is that a relatively moderate increase of size increases the magnitude of the magnetic field many times over. Figure 4 plots the measured intensity at 30 cm height for a defined set of magnets along the x-axis and the bell shaped curve can easily be seen. The curve is symmetric along the z-axis, as can be seen in Figure 5. The magnetic field depends on the dimensions of the magnet and a plot of the intensity at 30 cm for a set of dimensions is shown in Figure 6. A diameter can be selected, e.g. 2 cm, and intensity, e.g. 100 µT, and then it can be deduced that the magnet needs to be about 5.4 cm in length to have this intensity at this height. It is also possible to select a given intensity and then follow the corresponding graph and select a magnet that fits these parameters.

More graphs are included in the appendix in section 11.1.

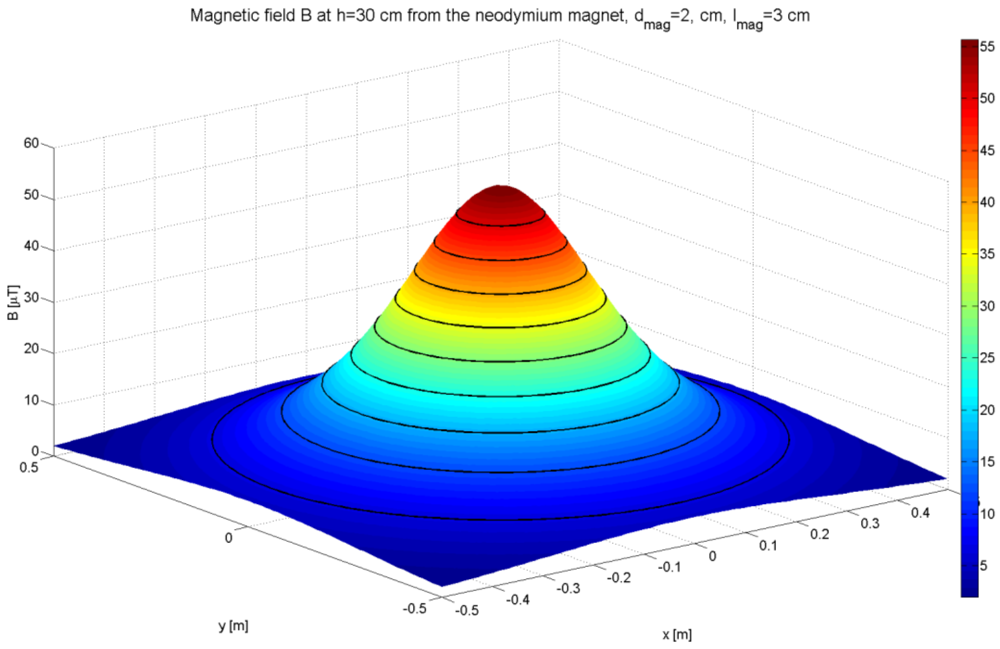

Figure 5 A 3D plot of the magnetic field from a 2×3 cm neodymium magnet as measured on a height of 30 cm

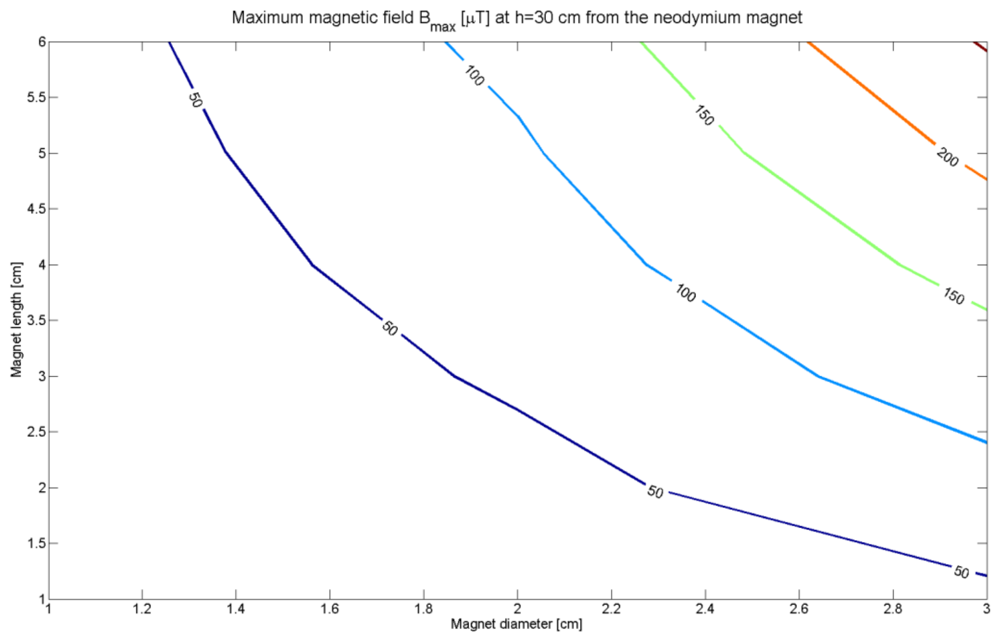

Figure 6 Study of the magnetic field as a function of the magnet's dimensions

3.2.1.2 The magnetic field in free space with a layer of asphalt

The detected intensity at a given height not only depends on the magnet itself but also the surrounding materials. The environment around the magnet can be considered as free space as long as the relative magnetic permeability μ_r of the materials around it is close to 1. In such an environment there are no distortions of the magnetic field. If there are any materials around the magnet that has a relative magnetic permeability larger than 1, this will produce sizable distortions of the magnetic field. A model has been developed following the approach of [3] to estimate how the magnetic field could be affected by the presence of ferromagnetic impurities in the asphalt layer.

As long as the material has no magnetic properties – i.e. the materials μ_r is sufficiently close to 1 – then the material can be treated as air for this purpose. If the material has some magnetic property, then the field will be affected. A model has been developed that assumes that all magnetic properties are located in the asphalt and the layers beneath this have no magnetic properties, see Figure 7.

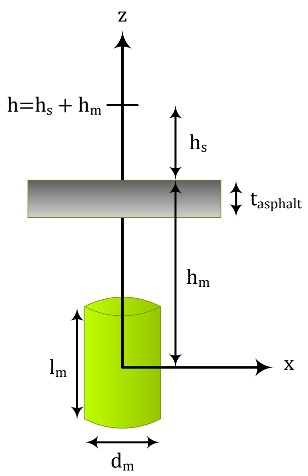

Figure 7 Parameter definition for parametric study in free space with a layer of asphalt

The magnetic properties of the material in the Swedish road network is unknown, as this has not been a parameter when the material has been selected or quality controlled. The magnetic properties of a material with magnetic impurities are studied in [3], and a study has been performed to understand how the magnetic field is affected by a layer of asphalt with magnetic impurities. This study was performed using finite element method analysis in COMSOL [4] instead of the dipole model.

From [3] a μ_r from 1 to 20 has been studied, see Figure 8, and when a very high μ_r is used, the magnetic field is down to a third of the original field. Figure 9 and Figure 10 shows how the magnetic field behaves in the two extremes, μ_r=1 and μ_r=20. The asphalt layer is 10 cm thick and located at a height of 5 cm from the centre of the magnet.

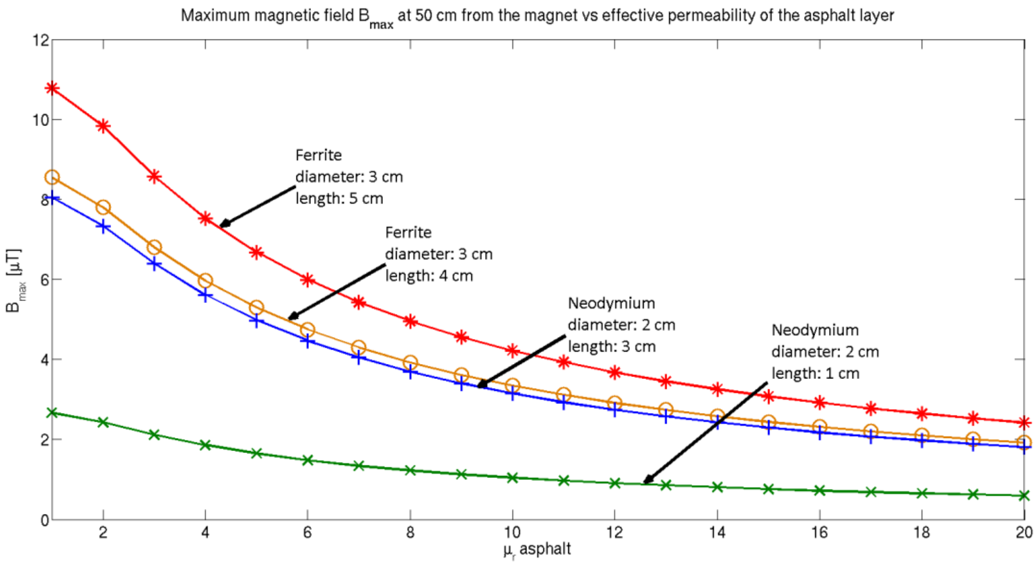

Figure 8 The magnetic field as a function of the magnetic properties of the asphalt layer

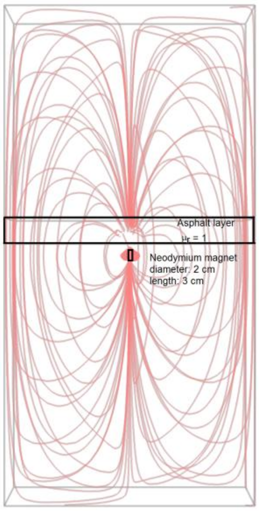

Figure 9 Magnetic field lines for a 2×3 cm Neodymium with asphalt layer with μ_r equal to 1

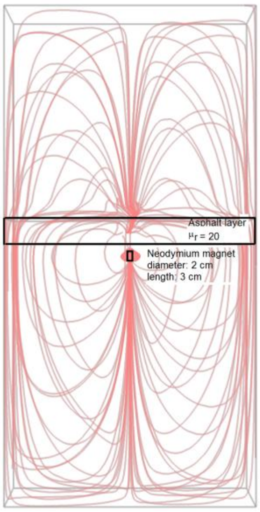

Figure 10 Magnetic field lines for a 2×3 cm Neodymium with asphalt layer with μ_r equal to 20

3.2.1.3 The magnetic field in free space with a steel sheet

The body and the chassis of the vehicle are mainly made from metal and the metal content close to the sensor is very high. This will alter the magnetic field and to study the influence a simple model was developed. A five millimetre thick homogenous steel sheet was located above a 3×5 cm ferrite magnet, the height of the sheet was varied and the magnetic field was calculated at a point 50 cm above the centre of the magnet. This means that with the definitions of Figure 11 the height h is 50 cm and z_{pl} is varied between h±30 cm, that is z_{pl} = [20, .., 80] cm. The measured field B at height h is plotted in Figure 12. The distance between the sheet and the sensor is denoted Δz_{pl}, a Δz_{pl} of zero means the sensor is inside the sheet. This study was performed using finite element method analysis in COMSOL [4] instead of the dipole model.

The steel sheet leads the magnetic field lines as in the case with the asphalt layer in Figure 10 and the sensor detects a more intense magnetic field close to the sheet. The field is distorted relatively to the bell-shaped distribution detectable in free space and this will likely make it harder to accurately detect the location of the magnet. This needs further study and a more accurate model of the vehicle than a steel sheet needs to be developed.

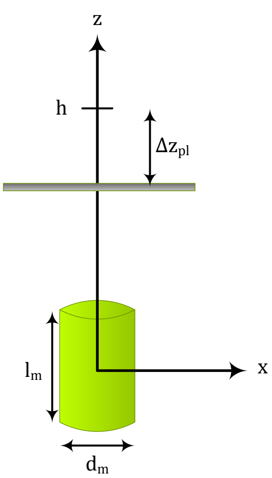

Figure 11 Parameter definition for parametric study in free space with a steel sheet

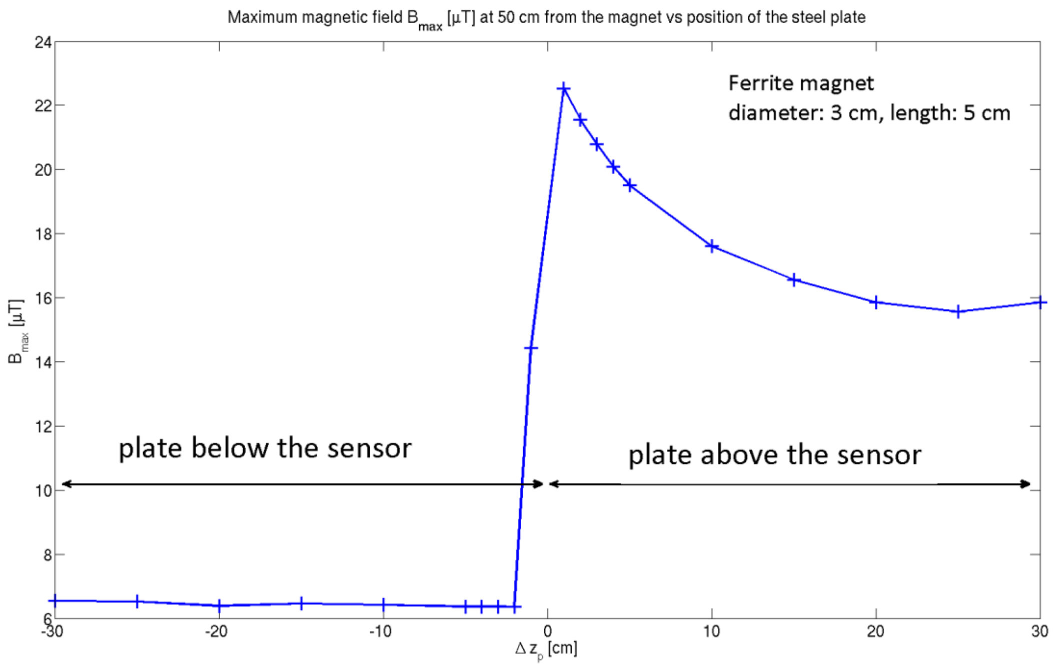

Figure 12 Magnetic field at 50 cm as a function of the distance from a five millimetre thick steel sheet

3.2.2 Temperature-dependence of the magnets

All calculations in this report are done at room temperature (20-23°C) and the literature reports all magnetic constants at this temperature, but the magnetisation varies with the temperature. The magnetisation of the magnet is affected in one of three ways due to temperature:

1. Reversible losses – losses of magnetic flux that are reversed once the magnet is returned to room temperature.
2. Irreversible losses – losses of magnetic flux that are not reversed once the magnet is at room temperature, the magnet has become weaker. The magnet can (theoretically) be “repaired” by applying a sufficiently strong external magnetic field.
3. Permanent losses – the magnet is demagnetised and cannot be “repaired” since the internal atomic structure has changed because of the temperature.

Every magnetic has a maximum operational temperature, $T_{op,max}$, that depends on a number of parameters, the geometrical shape of the magnet being one. The theory behind the calculations are quite complex but there exist tools that can be used to calculate a maximum operational temperature for a given magnet. This is usually not necessary as the supplier gives $T_{op,max}$ for the supplied magnets. Another temperature property of a magnet is the Curie temperature, T_{Curie}, at which the magnet is permanently demagnetised. For the magnets used in this report these temperatures are reported in Table 1 below.

Magnet type	$T_{op,max}$	T_{Curie}	Temperature Coefficient (B_r)	Breakdown temperature
Neodymium, N35	80°C	300°C	-0.11%/°C	900-1000°C
Ferrite, Y30	250°C	450°C	-0.19 %/°C	Information not found

Table 1 Temperature constants for magnets

A magnet that is exposed to temperatures up to $T_{op,max}$ might gain reversible losses, but will return to the normal intensity once the magnet is returned to room temperature. If the magnet is exposed to temperatures above the maximum operational temperature it will lose some of its magnetisation and will be weaker once returned to room temperature. How much weaker depends on the temperature and a number of complex parameters far beyond the scope of this report.

A magnet that is heated to its Curie temperature loses all of its magnetisation properties but once it is cooled down some of it is regained. A permanent loss of magnetisation requires quite extreme temperatures, the *Breakdown temperature* reported in Table 1. Note that reliable information for ferrites has not been found, this is a constant that depends on the design of the magnet and the manufacturing process and is quite hard to calculate as all parameters aren't openly reported by the manufacturers.

The magnetic field is proportional to the temperature with the temperature coefficient reported in Table 1. The higher the temperature, the lower the magnetic field intensity is and the lower the temperature, the higher the field intensity is.

This holds true for all temperatures that is relevant for this report but ferrites behaves a little different from neodymium at lower temperatures and it is not recommended to use ferrites below -60°C. Even a brief description of the physics is beyond the scope of this report.

For this report only the case of demagnetization due to high temperatures needs to be taken into account. The low temperatures that could weaken the strength of the considered magnets are never attained in reality.

3.3 Estimating the position of the vehicle

3.3.1 General problem statement

From a signal processing view the challenge is to find an optimal estimate of the vehicle position given measurements of the magnetic field, information about the position of the magnetic markers and the inertial reference platform of the vehicle.

Since the environment around the vehicle is to a high degree unpredictable and the accuracy of the sensors is limited by noise, a probabilistic approach is used to handle the uncertainty. Assuming a priori knowledge about the vehicle dynamics and the magnetic field from the magnets a Bayesian filter can be used to recursively estimate the vehicle position.

3.3.2 Choice of coordinate system

The choice of coordinate systems describing the measurements and the vehicle position is an important factor in the design of the signal processing algorithm.

In order to make the notation simple an earth bound Cartesian coordinate system is chosen. In this coordinate system the magnets are stationary and the vehicle is moving. The frame of reference for the measurements is bound to the magnetic sensor system in the vehicle and is also described by a Cartesian coordinate system. A transformation between the two coordinate systems can be obtained by translation and rotation.

In this report we use the word *longitudinal* in the meaning; the length direction of the vehicle and *lateral* in the meaning; the direction of the rear axle. These two directions are assumed to be orthogonal.

In this report we do not specify the coordinate system in focus unless it is necessary for the final conclusion.

3.3.3 Bayesian filter model

The goal of the filtering process is to recursively find an optimal estimate of the state vector considering all of the past measurements of the magnetic field. Define the vector X_k representing the complete state necessary to describe the dynamical system at discrete point *k* in time.

The state vector is assumed to evolve according to the state transition model:

$$\boldsymbol{X_{k+1}} = \boldsymbol{f}(\boldsymbol{X_k}) + \boldsymbol{v_k}$$

Equation 6 The state transition model

where the function $f()$ describes the motion of the vehicle and v_k is additive process noise including any effects or disturbances not taken care of in the motion model.

Let the measurement vector Z_k describe the measured magnetic field at time *k*. To simplify the notation the internal sensors of the vehicle, e.g. yaw rate, are not included in the measurement model but are instead treated as parameters in the state transition model. Hence the measurements carry information from the magnetic markers about the state vector via the measurement model:

$$\boldsymbol{Z_k} = \boldsymbol{H}(\boldsymbol{X_k}) + \boldsymbol{w_k}$$

Equation 7 The measurement model

where $H()$ is model of the total magnetic field at the sensor and w_k is the measurement noise. In special cases it is possible to find an analytical optimal estimate of the state vector X_k but in most real life situations H and F are non-linear and approximate filters such as e.g. the *unscented Kalman filter* are used.

3.4 Structure of the carriageway

The Swedish road network is currently built according to the standards set by [5], but roads built according to older standards are very common. The structure of a road consists of several layers, which materials and how thick each layer is depends on the type of road, traffic loading, local geotechnical properties and the standard the road was built according to.

The road will be affected by the traffic and by the change of seasons. The thawing in the spring will make some movements of the road layers but that is within limits [6] and is of little concern for the project. Large movements would damage the pavement and will need to be repaired.

The traffic will make ruts in the pavement, both due to compacting and wear. Allowed rut depth before the pavement is repaired depends on several factors but the limit is never more than 18 mm [6]. Most of the rut depth is due to wear and tear, and the layers beneath the asphalt rarely deforms once set [6].

The temperature below the carriageway depends on the air temperature, the wind velocity and the sun radiation [7] and experiments [8] shows that the temperature can fluctuate heavily. Further analysis needs to be performed but preliminary results shows that the temperature will only affect the magnets within acceptable limits (see section 3.2.2 and the analysis in section 6.4).

The case for tunnels and bridges is slightly different. There exist requirements – see [9] and [10] – which bridges and tunnels shall be built according to. The major differences that will affect the magnetic marker system is the depth that the marker can be buried, the movements of the road and the construction's interference with the magnetic field. The movement is not expected to exceed that of an ordinary road; it is even expected to be less for both bridges and tunnels.

The maximum depth of a marker depends on the design of the bridge or the tunnel; it is expected from [9] and [10] that it is deeper for tunnels than for bridges. How deep a marker needs to be buried is mandated by the amount of protection the marker needs from the wear of the carriageway by the traffic, the movements of the road structure and road maintenance.

The traffic's wearing and the movements of the carriageway have already been defined to be small and the depth due to road maintenance is the same as for ordinary roads. This means that the marker can be buried at the same depth as in an ordinary road, but for some bridges and tunnels a smaller depth has to be used. How much smaller depends on the individual bridge or tunnel. As long as the road maintenance doesn't interfere with the magnet this should not be a problem. Alternative magnets might be needed on specific bridges and in specific tunnels.

The construction of both tunnels and especially bridges involves a large amount of rebar construction, which will interfere with the magnetic field. An analysis needs to be performed for each individual type of tunnel and bridge to be able to find a solution. It is not possible to define a general solution as the construction can vary greatly between types.

3.4.1 Road maintenance

Part of the old asphalt is usually removed before new pavement is applied to a road. How much depends on the quality of the old asphalt, the annual average day traffic etc. The higher the demands on the road, the more invasive the repair and reconstruction can be. The usual approach is to mill the asphalt layer and according to [6] this is usually done to a depth of between 20 and 100 mm. On top of the milled surface a new asphalt layer is spread and the thickness can vary greatly, but almost never more than 150 mm.

If the same standard is used for a road equipped with magnetic markers as for current roads, then the distance between the marker and the sensors can increase with several centimetres over time for the same length of road and the top of the marker need to be at least 15 cm beneath the surface. A depth of 20 cm for the centre of the magnet is recommended for a sufficient margin.

4 In-vehicle system design

A prototype system was implemented which could detect the magnetic markers and estimate the position of the vehicle. In this section the design of the system is presented.

4.1 Logical design

The in-vehicle system was designed as two parts; a data acquisition system and an analysis system. The former was a system that acquired the sensor data and logged it together with other relevant data from the vehicle. The analysis system was developed in Octave [11] and performed the analysis on a separate PC; the analysis was not performed in real time. See Figure 13 for an overview of the system.

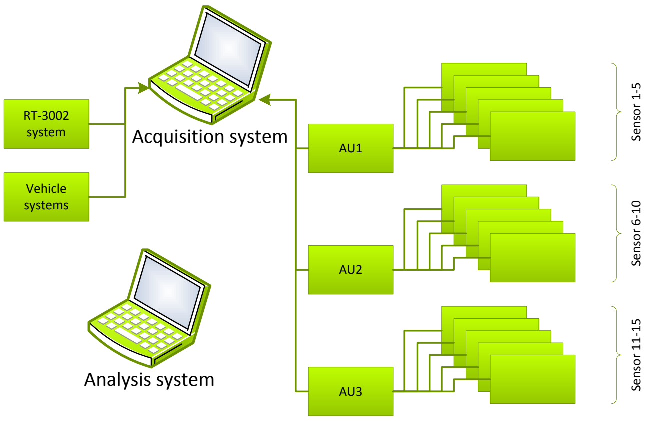

Figure 13 System overview

Each part is further described in the following sections.

4.2 Data acquisition system

To be able to measure the magnets and feed logging data to the algorithm an acquisition system was developed. It consisted of three parts: a sensor array, data acquisition units and a laptop that logged the resulting CAN data together with other CAN signals from the test vehicle, e.g. the odometer and the speed. A RT-3002 system [12] was used to log the vehicle's absolute position for reference with an accuracy of approximately 5 cm in the specific setup.

Figure 14 The sensor system mounted on the test vehicle's tow ball, with the sensor array seen in the smaller grey boxes beneath the beam holding the acquisition units. The grey cable from the trunk is the power supply to the system and the CAN bus.

The sensor array consisted of a total of fifteen modules with one Honeywell HMC1053 three axis magnetoresistive sensor [13] in each. Five sensor modules where connected to one acquisition unit (AU), based on a STM32F4 DISCOVERY board [14], and the analogue signals for each axis were sampled and converted to a 12 bit digital value using the board processor's internal analogue to digital converter (ADC). The ADC had sixteen channels so it could only handle five sensors (three axis times five sensors requires fifteen channels) so a total of three subsystems had to be used. Fifteen sensor modules were used to log as much data as possible to be able to answer as many of the research issues as possible. See Figure 14 for a picture of the sensor array and the three acquisition units (the larger grey boxes).

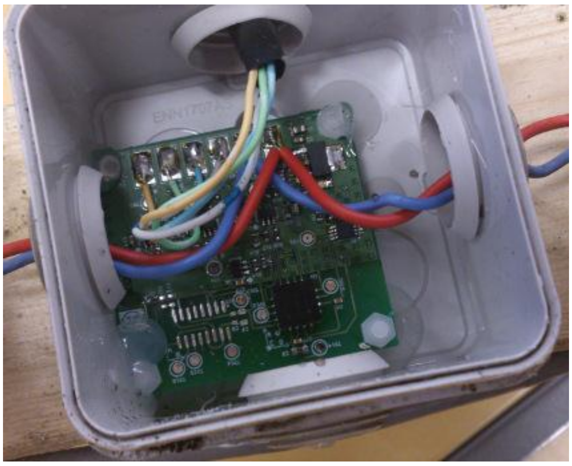

Figure 15 The sensor module, the sensor chip is in the lower right corner of the PCB

The resulting data was transmitted over the sensor system's CAN bus at 1 Mbit/s using standard CAN frames and logged by a laptop that also logged relevant CAN signals from the vehicle (e.g. vehicle speed) and the reference positioning system. The sampling rate was about 500 samples per second. The system was able to sample the AD-converters faster but as focus was on getting a large amount of data the bandwidth of the CAN bus set some limitations on the number of samples. The sampling rate can easily be increased by decreasing the number of bits used by the ADC, the number of axis and of course reduce the number of sensors.

4.3 Sensor requirements

Preliminary simulations early in the project of the magnetic field using FEMM [15] indicated that a passing vehicle would have quite a short distance where the field would be detectable. These preliminary calculations were found to be consistent with other findings [16]. Since one of the requirements of the system was to be able to detect magnets at 150 km/h, which is 41.7 m/s, a sampling rate of at least 400 samples per second was required which made the selection of sensors challenging. Most magnetic sensors are Hall sensors which are designed to detect a small magnet at a very close distance (usually a few centimetres) at sampling rates of just a few samples per second.

Some sensors are designed to detect the Earth's magnetic field. These can fall into two categories, either chips designed to act as compasses in e.g. mobile phones or products designed for industrial use. The former usually has a maximum sampling rate of 80 Hz and the latter were too expensive when a suitable sensor was found.

The magnetoresistive sensors from Honeywell, with the family of chips described in [13], were chosen. Table 2 below gives a few of the evaluated sensors and the reasons for rejections; the chosen sensor HMC1053 is included for reference.

Manufacturer	Model	B_{MAX}	Sensitivity	Sampling rate/ Bandwidth	Approx. price (SEK)	Comments
Stefan Mayer	FLC3-70	200 µT	1 V/35 µT	1 kHz	4300	
Freescale	MAG3110	1 mT	100 nT	80 Hz	7.50	
Honeywell	HMC1022	6 mT	120 nT	5 MHz	50	Two axis
Honeywell	HMC1053	6 mT	120 nT	5 MHz	330	
Crossbow	CXM539	100 µT	100 nT	200 Hz	Unknown	

Table 2 A selection of sensors for comparison, red cells marks the reason for rejection.

The HMC1053 was selected since it very much was the only sensor that would be able to detect the magnets at the required speed. The HMC1022 was also a candidate but as the primary objective for the acquisition system was to collect data a three axis sensor was chosen.

4.4 Signal Processing

The logging data from the acquisition system was fed into an application developed in Octave [11], for practical reasons running on a separate laptop. The analysis was not performed in real time.

4.4.1 General algorithm design

Due to the fast decay of the magnetic field intensity the measurements only have a high SNR close to the markers. Hence, for vehicle positioning between the markers dead reckoning is used. Since the markers are assumed to be placed at a relative long distance from each other compared to the fast decay of the magnetic field intensity, the general algorithm can be split into two parts without loss of generality in the analysis of the research questions in this project.

1. global positioning close to the markers using information in the magnetic field
2. relative positioning between the markers using dead reckoning

In an application, where only the total positioning error is relevant, these two estimates should be fused using e.g. a Bayesian filter, see section 3.3.

The dead reckoning positioning error depends on the inertial sensor configuration of the vehicle but is considered well known. Hence an algorithm was developed to estimate the vehicle position error both in simulated environment and using measured data. The algorithm focused on estimating the vehicle position using only information from the magnetic markers i.e. measured field intensity and the global position of the magnetic markers. A *non-linear least squares* (NLS) approach was then applied to find the vehicle position that minimizes the quadratic error of the difference between the measurements and the predicted field intensity described by the model in Equation 7.

5 Experiments

5.1 Test Methods

To verify the system performance with real data a test course was built and the vehicle was driven along this course a large number of times in various configurations. The goal was to measure the noise in the measured data, gather data on how the sensors measured the magnetic field and have valid data to feed to the analysis application.

For practical reasons there were two test courses, both situated at Hällered Proving Ground near Gothenburg, one low speed and one high speed test course. The low speed test track was a forest road where it was easy to insert the magnets at various depths; the maximum practical speed was 70 km/h. The high speed test field was a large paved field where it was possible to safely drive at speeds in excess of 150 km/h.

The measured data was logged together with the vehicle's data and the vehicle positioning reported by the RT-3002 system.

5.2 The low speed test track "The Forest Road"

The test track was a several hundred meters long forest road consisting of a layer of stones of various sizes and on top of that a thick layer of soil had formed over the years. The road was quite slippery after rainfall but not so much that it interfered with the measurement plan. Because the road was uneven and the vehicle's suspension made the sensor ramp swing, the speed limit was for practical and safety reasons set to 70 km/h.

Figure 16 The Forest Road test track, the road cone marks the beginning of the track, as shown with a yellow dot in the middle of the road. A similar road cone might be seen in the distance before the high spruce marking the end of the track.

The magnets were inserted in the road surface along a 120 meter long test course in the middle of the road. A plastic pipe had been cut to the desired length and the magnets were placed inside this pipe, Figure 17. The pipe was then inserted in the road so that the top end was levelled with the road surface. The top end was painted yellow to make it possible for the driver to see them but it only took a few test runs before the markers were covered in debris, instead marking spray paint was used on the road itself. The positions of the individual magnets were measured using a RT-3002 system [12] for later reference.

Figure 17 A selection of "magnetic pipes"; two 6 cm and one 24 cm white pipe for neodymium magnets and 10 cm, 25 cm and 35 cm long pipes for ferrite magnets. A 3 cm neodymium magnet and a 3 cm ferrite magnet are included to the left for reference.

The majority of the measurements were performed on this track and many different test cases were used to gather as much data as possible under different circumstances. The vehicle was driven at various fixed speeds, from just a few kilometres per hour up to 70 km/h. The positioning of the vehicle relative to the magnets was varied; in the middle and to the left and right, and from one side to the other in an S-form. Finally the speed was varied during the measurement, e.g. from 20 km/h to 60 km/h and then down to 20 km/h again during the test track's 120 meters.

Two kinds of magnets were used, all cylindrical with the magnetisation in the height direction. The type mostly used was neodymium magnets 20 mm in diameter and 10 mm thick. The other type was ferrite magnets 30 mm in diameter and 5 mm thick. These were arranged in stacks at various lengths, e.g. a 5 cm neodymium magnet is five 2×1 cm magnets arranged into one cylinder of 2×5 cm. the used neodymium magnets where of N35 quality and the ferrites were of Y30 quality. The latter corresponds to HF26/18 according to IEC 60404-8-1.

The depth of the magnets is defined in this section as the distance from the road surface down to the top of the magnet. The depth of the hole, and hence the length of the plastic pipe, is the depth of the magnet plus the length of the magnet itself.

The first 100 meters consisted of 100 neodymium magnets at zero depth and at a length of 6 cm. This length was varied; measurements were performed on 1, 3 and 6 cm lengths. As the magnet was located at the bottom of the pipe, the depth of the magnet increased equally with the decrease of the length (a 3 cm magnet was at a depth of 3 cm, a 1 cm magnet was at a depth of 5 cm). The magnetic polarity of the magnets was mostly but not always alternating, i.e. the north pole of the magnet was directed upwards on every second magnet and downward on every second magnet. This was varied between some of the tests.

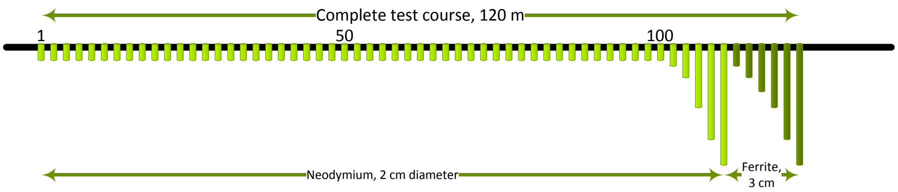

Figure 18 Side view of the magnetic markers inserted in the forest road, only every second marker is show, the figure is not to scale.

The next ten magnets were 4 cm neodymium magnets at an increasing depth, from 5 cm down to 50 cm. This was to get a reference on how the depth of the magnet affected the magnetic field. Then the final ten magnets were 10 cm Ferrite magnets at an increasing depth from zero down to 50 cm. See Figure 18 for a simplified side view, the magnets shown in the figure is not to scale and only every second magnet is shown.

5.3 The high speed test field

Due to safety reasons a special area had to be used for the high speed measurements. Hällered Proving Ground consists of an area which can be cordoned off and is large enough for it to be safe to drive at these speeds – and where it is legal to drive a car at far beyond the ordinary speed limit.

For these tests the objective was to measure the bandwidth of the system and therefore there were no need to inject the magnets into the carriageway, nor vary the intensity of the magnets. A fifty meter long test course was used with a two centimetre in diameter and one centimetre high cylindrical neodymium magnet one meter apart. The magnets were glued to the road surface to make sure the magnets did not move–or even were caught by the vehicle–when the vehicle passed, see Figure 19.

Figure 19 Gluing the magnets to the pavement for the high speed test, the torch was used for drying the pavement.

The test plan included various speeds from 100 km/h up to 165 km/h and the vehicle was positioned relative to the magnets at three different positions; with the magnets in the middle under the car, with the magnets to the side under the driver's seat and the magnets to the side under the passenger's seat. Five additional tests were performed where the driver braked when the vehicle arrived at the test course. These five tests are as follows (the reaction time by the driver made the brake position to vary a bit, all speeds below were measured by the driver keeping an eye on the speedometer in the cluster when the first and the last magnet was passed):

1. Braking when arriving at the first magnet from 130 km/h down to 110 km/h, i.e. so called light braking.
2. Braking when arriving at the first magnet from 130 km/h down to 95 km/h, i.e. so called heavy braking.
3. Braking slightly before arriving at the first magnet from 130 km/h down to 110 km/h, i.e. so called light braking.
4. Braking slightly before arriving at the first magnet from 130 km/h down to 95 km/h, i.e. so called heavy braking.
5. Braking when arriving at the first magnet from 150 km/h down to 130 km/h, i.e. so called light braking.

The exact speed reported by the vehicle on the CAN bus was logged for later reference.

6 Analysis

6.1 System performance

6.1.1 Signal and noise

The analogue-to-digital converter, ADC, has twelve bits and a signal span of 3 volt. Magnetic field intensity is measured in tesla, denoted T. The conversion factor $\frac{volt}{tesla}$ is approximately 3000 in the measurements.

The power of the signal from the markers and the noise is measured in tesla. Strictly, it is tesla squared, T^2, which is proportional to the power in watt. Define a unit dBµT that is read decibel micro tesla. If we have a value a in tesla, value a in dBµT is given by $20\log(a/10^{-6})$.

The magnetic field of a magnetic dipole in z-direction is given by function B_z in Equation 4. The decay of the field strength, $B_z(x,y,z)/B_z(0,0,z)$, depends on *x*, *y* and *z*, where z is the distance between the magnetic sensor and the marker's origin. For *z*=0.3 m, the -10 dB decay is when $r = \sqrt{x^2 + y^2} =$ 0.2 m. For *z*=0.5 m, we get that r is equal to 0.34 m.

For the magnetic sensor array with 15 sensors 0.1 m apart, the distance between sensor 1 and sensor 15 is 1.4 m. To obtain the signal power from one marker at *z*=0.3 m, we integrate $abs^2(B_z)$ for $x \in (-0.2, \dots ,0{,}2)$, $y \in (-0.7, \dots ,0{,}7)$. For *z*=0.5 m, we integrate over $x \in (-0.34, \dots ,0{,}34)$, $y \in (-0.7, \dots ,0{,}7)$. Table 3 shows the signal power for five different configurations of marker material, size and distance used in this section. These powers are from theoretical calculations but are good enough estimates of the signal power in the measurements.

Material	Diameter (m)	Length (m)	Sensor to marker origin (m)	Sensor to marker top (m)	Signal power (dBµT)
Neodymium	0.02	0.06	0.29	0.26	32.5
Neodymium	0.02	0.03	0.305	0.29	25.5
Neodymium	0.02	0.01	0.315	0.31	15.4
Ferrite	0.04	0.015	0.3175	0.31	22.4
Ferrite	0.04	0.015	0.5075	0.5	12.0

Table 3 Signal power for different marker size, material and distance sensor to marker

6.1.2 Measurements

Figure 20 to Figure 22 shows magnetic sensor data from measurements on the forest road at 30 km/h. The first 100 markers were all 2×1 cm neodymium magnets. The y-axis is the magnetic sensor output in volt and the x-axis is the relative odometer since start. In Figure 20, there is roughly 90 meters of only noise before reaching the first magnet.

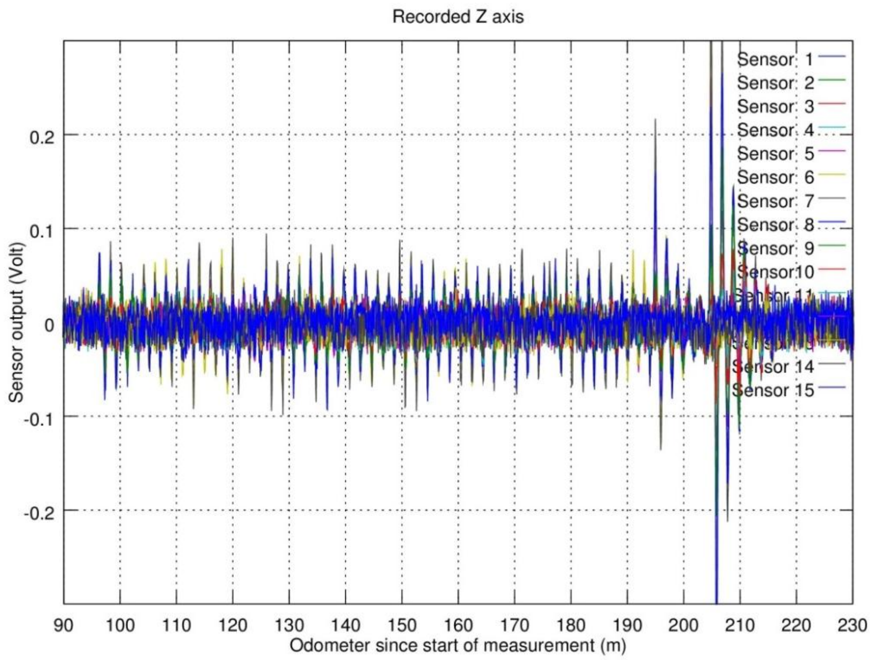

Figure 20 Output from magnetic sensor in volt when vehicle has travelled 90 to 230 meters since start

Figure 21 shows the odometer between 90 and 140 meters and the first marker has north pointing up. The orientation of the second marker has south pointing up. The orientation changed north, south, north, etc. for the first 100 markers. The forest road was bumpy and since the magnetic sensor array was 1.2 m behind the rear-axis, any change in pitch or roll affects the received signal. This can be seen in the figure below where the amplitude changes.

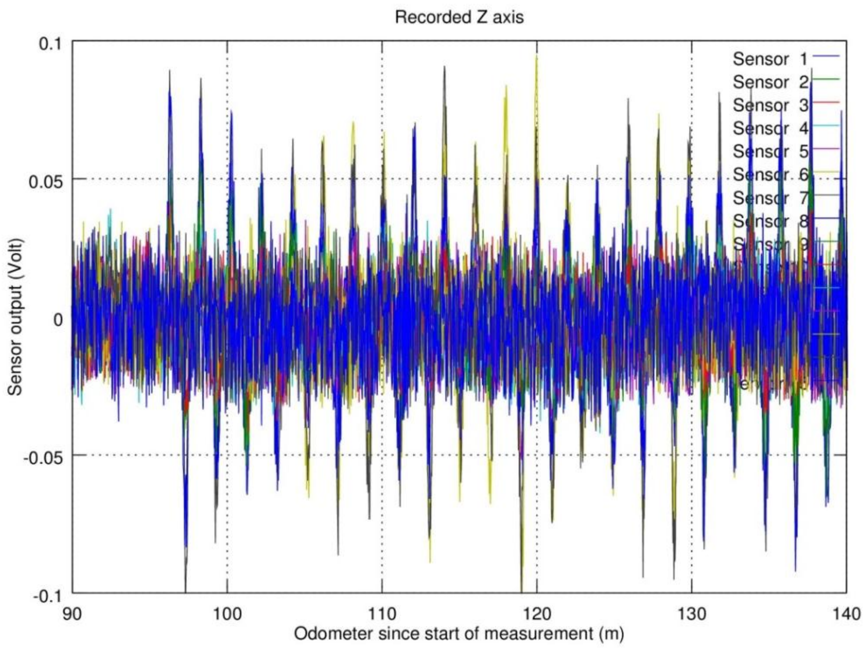

Figure 21 Output from magnetic sensor in volt when vehicle has travelled 90 to 140 meters since start

In the Figure 22, we view the data in lateral direction for every sensor. Sensor 1 has a lateral position of -0.7 m in the vehicle's coordinate system. Sensor 2 is at -0.6 m, sensor 3 at -0.5 m, etc. Sensor 8 is at 0 m, and sensor 15 is at 0.7 m.

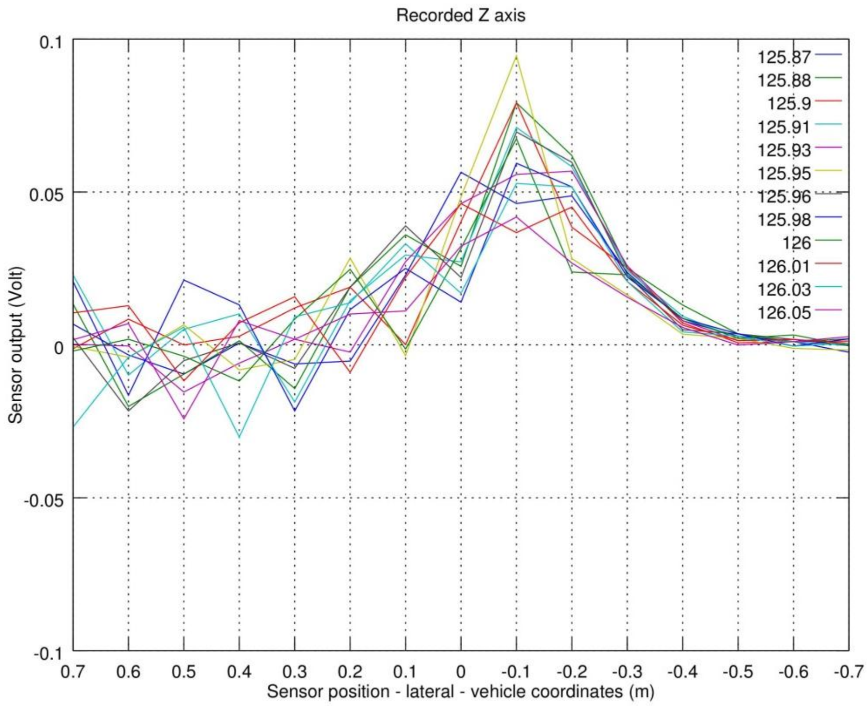

Figure 22 Sensor output for all 15 sensors. Note the difference in noise level between sensor 1-10 and sensor 11-15 is due to noise on the common power cord feeding the ACU units.

There are three AU units, each sampling from 5 sensors. The noise is much higher for AU2 with sensor 6 to 10 and AU3 with sensor 11 to 15 compared to AU1 with sensor 1 to 5. During the first 80 m, the noise level for AU1 to AU3 was estimated to be 1, 14 and 15 dBµT, respectively. The noise level was independent of speed. The noise level of one sensor in the lab was -3.5 dBµT.

The main reason is the power supply construction. The external power supply is connected to AU1. Then, AU2 gets its power from AU1 and AU3 gets its power from AU2. An AU supplies power to its ADC and its five magnetic sensors. It turned out that the DC/DC conversion in every AU sent out a lot of noise on the common power cord that then affected the next AU down the line. By adding analogue filters the noise level was lowered before the high-speed measurements for AU1, AU2 and AU3 to be -5, -4 and -2 dBµT, respectively.

At the last day of measurements, the magnetic sensor array was mounted just behind the front wheels. The purpose was to measure the noise level. The magnetic sensor array has not been designed to be mounted there with particular shielding from electric and magnetic disturbances. At speeds up to 40 km/h, we measured a noise level of 20 – 21 dBµT. At 60, 70, 80, and 90 km/h, we got approximately 16, 18, 15, and 9 dBµT, respectively. This measurement has not been extensively analysed. This indicates that the installation in the vehicle is crucial to the noise level. Further investigation is needed to determine the noise level for a sensor array designed for vehicle installation.

6.1.3 Estimated positioning error – forest road simulation

Only results from simulations are presented in this section with a straight road with 100 markers. The setup is the same as the measurements from the forest road. There are 15 magnetic sensors mounted 10 cm apart. The following marker configurations from Table 3 are used:

1. Neodymium 2x6 cm, z = 26 cm, S=32.5 dBµT
2. Neodymium 2x3 cm, z = 29 cm, S=25.4 dBµT
3. Neodymium 2x1 cm, z = 31 cm, S=15.4 dBµT
4. Ferrite 4x1.5 cm, z = 31 cm, S=22.5 dBµT

S is the signal power and z is the smallest achieved vertical distance between a magnetic sensor and a marker. The distance is different for the different configurations in forest road measurements. All are around 30 cm since the magnetic sensor array was roughly 26 cm above ground. The noise N is unbalanced and is 1, 14, 15 dBµT for AU1, AU2 and AU3, respectively. In general, the SNR in dB is given by S - N. Further, SNR is often a good indicator of achieved performance. However, due to the unbalanced noise, it is tricky to get one SNR number here that indicates the performance of the algorithm. The ferrite marker configuration was not used in the forest road measurements but is included here since it is the recommended choice.

In Figure 23 and Figure 24, the longitudinal and lateral RMS error is presented. Using the largest 2x6 cm neodymium magnet gives an error that is zero or almost zero. This is due to the high signal power of 32.5 dBµT. The RMS increases up to 1.3 cm when the signal power is decreased down to 15.4 dBµT.

An update to the global position is done at 500 Hz, same as the sampling rate of the magnetic sensor array. When sampling the magnetic sensor array, fifteen samples are obtained in the lateral direction but only one in the longitudinal direction. The lateral resolution is always 10 cm. The longitudinal resolution decreases with higher speed since fewer samples per decimetre is obtained within the 20 cm threshold. At 50 m/s or 180 km/h, one sample per 10 cm is obtained. At 5m/s or 118 km/h, one sample every 1 cm is received. A decrease in resolution gives larger errors. The lateral and longitudinal errors are correlated, normally. This explains why both the longitudinal and lateral RMS error increases with increasing speed.

These curves will be compared below with the corresponding curves with the measured data from the forest road. The simulated environment provides the true speed and heading to the tracking algorithm. Thus, the dead reckoning error is always zero.

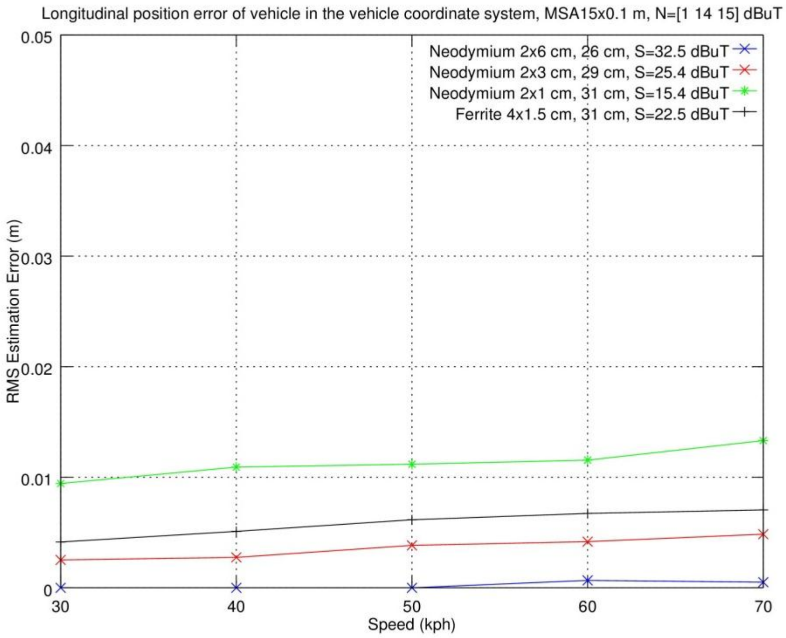

Figure 23 RMS error of the position estimate in the vehicle's longitudinal direction, x, using simulated magnetic sensor data for 15 sensors 10 cm apart with noise = 1, 14, 15 dBμT for AU1, AU2, and AU3.

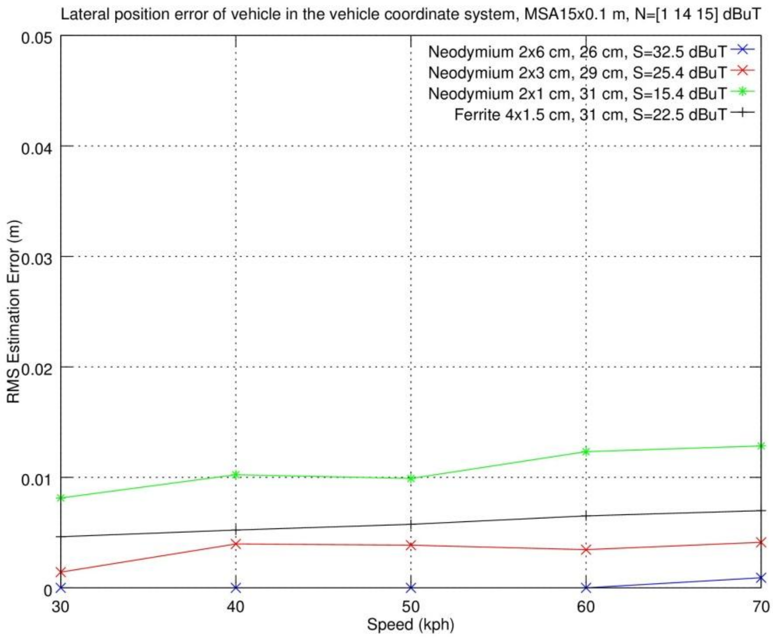

Figure 24 RMS error of the position estimate in the vehicle's lateral direction, y, using simulated magnetic sensor data for 15 sensors 10 cm apart with noise = 1, 14, 15 dBμT for AU1, AU2, and AU3.

6.1.4 Estimated positioning error – simulation with 50 cm and different noise levels

The proposed magnet is a 4x1.5 cm ferrite. In the section above, the vertical distance is about 30 cm. A more realistic distance is about 50 cm, see section 6.2. A ferrite of 4x1.5 cm at 50 cm height gives a signal power *S* equal to 12 dBµT. In this section all AUs have the same noise *N* and the SNR is 12-*N* dB. Results are presented for two configurations of magnetic sensor arrays, 15 sensors 10 cm apart and 7 sensors 20 m apart. The purpose is to study the effect of decreased number of sensors to reduce the cost and complexity of the system. All results in this section are from simulations with a straight road and 100 markers. Since the simulated environment provides the true speed and heading to the tracking algorithm, the dead reckoning error is always zero. With only 100 markers, a limited set of statistics is obtained. This explains why the lines are moving a bit up and down at higher noise levels.

In Figure 25 – Figure 28, the longitudinal and lateral RMS error increases when the noise increases from 1 to 16 dBµT or SNR decreases from 11 to -4 dB. In general, the error is almost the same for longitudinal and lateral for same speed and noise level. At 120 km/h, for a 15x10 cm array, the error increases from almost 1 cm to 3.5 cm. For the 7x20cm array, the error increase from 1 to almost 5 cm at 120 km/h. The error increases around 20 – 25 % when the number of magnetic sensors is changed from 15 to 7. In all cases, the RMS error is less than the required 10 cm at SNR equal to 12-16 =-4 dB.

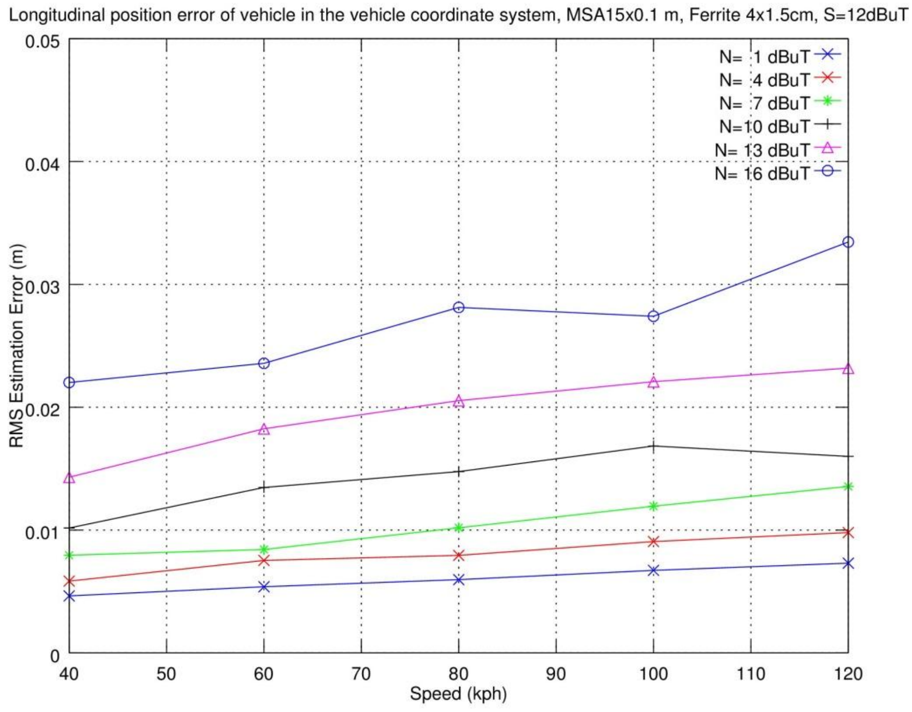

Figure 25 RMS error of the position estimate in the vehicle's longitudinal direction, x, using simulated magnetic sensor data for 15 sensors 10 cm apart with a distance sensor to marker of 50 cm

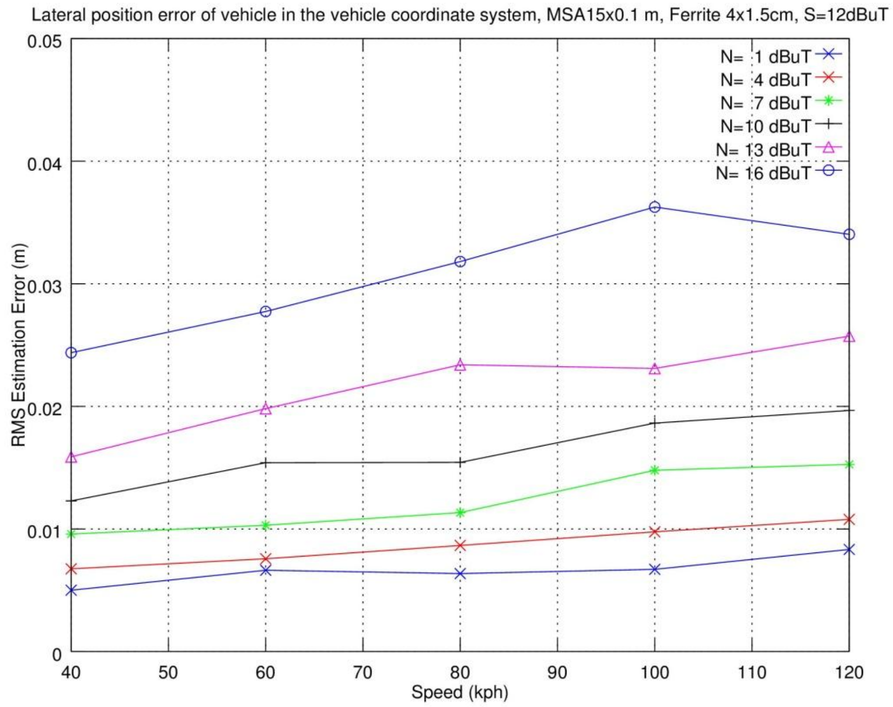

Figure 26 RMS error of the position estimate in the vehicle's lateral direction, y, using simulated magnetic sensor data for 15 sensors 10 cm apart, with a distance sensor to marker of 50 cm

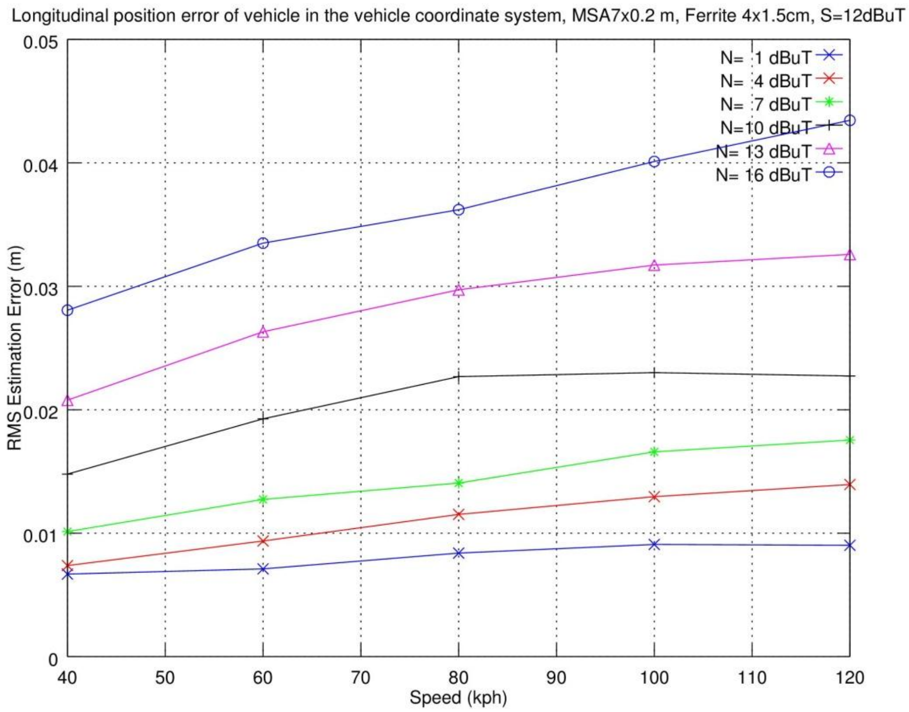

Figure 27 RMS error of the position estimate in the vehicle's longitudinal direction, x, using simulated magnetic sensor data for 7 sensors 20 cm apart, with a distance sensor to marker of 50 cm

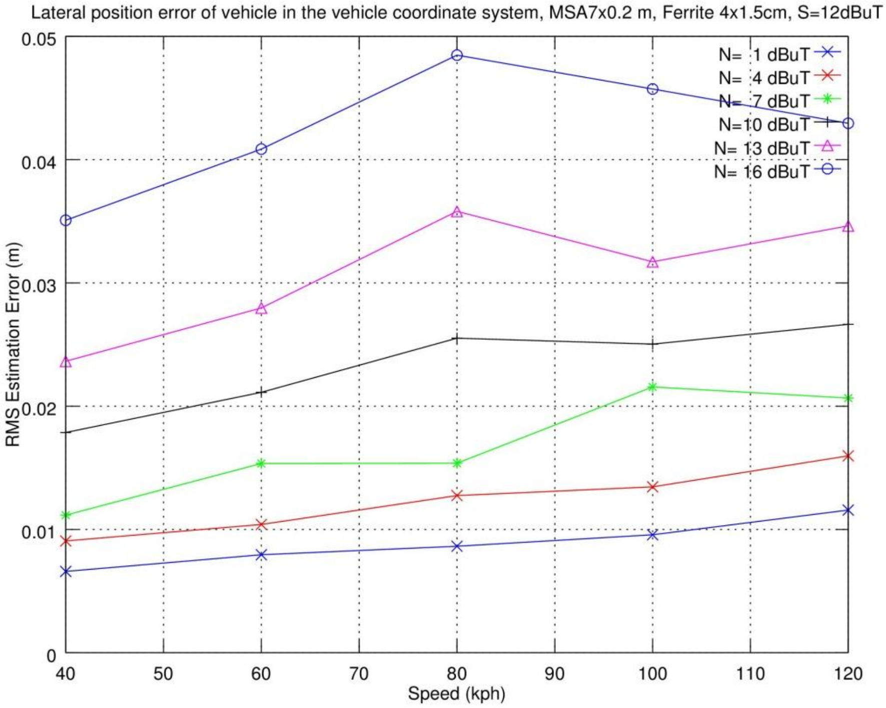

Figure 28 RMS error of the position estimate in the vehicle's lateral direction, y, using simulated magnetic sensor data for 7 sensors 20 cm apart, with a distance sensor to marker of 50 cm

6.1.5 Estimated positioning error – forest road measurements at 30 cm

In this section, results from running the tracking algorithm on forest road measurements are presented. The noise was 1, 14, and 15 dBµT for AU1, AU2, and AU3, respectively. The magnetic sensor array has 15 sensors 10 cm apart. It was only the first 100 markers that were changed between different measurements. The following marker configurations from Table 3 are used:

1. Neodymium 2x6 cm, z = 26 cm, S=32.5 dBµT
2. Neodymium 2x3 cm, z = 29 cm, S=25.4 dBµT
3. Neodymium 2x1 cm, z = 31 cm, S=15.4 dBµT

The estimated RMS error uses only the first 100 markers of the forest road. The lines in the figures below are moving a bit up and down. This is due to the fact that data from only 100 markers is available that gives limited statistics.

The tracking algorithm has two states:

1. Update position using measurements from magnetic markers
2. Update position using dead reckoning

When at least one magnetic sensor is closer, horizontally, than 20 cm to any marker, the algorithm is in state 1, otherwise 2. The 20 cm threshold is selected since magnetic field has its -10 dB decay at 20 cm, defined in section 6.1.1.

The purpose is to obtain the performance when the algorithm is in state 1. The simulated curves above do not have any dead reckoning error included since the simulated environment provides the true speed and heading to the tracking algorithm. The algorithm was altered so that the position error was saved when leaving state 1 and entering state 2 dead reckoning. When algorithm entered state 1 again, the position of the vehicle was set to the position given by the RT-3002 GPS plus the saved position error.

Figure 29 shows the longitudinal RMS error. The RMS error is around 13 cm for all three marker dimensions. Figure 30 shows the lateral RMS error between 2 to 8 cm. The lateral error is lower than the longitudinal error since the algorithm was tuned to provide lower lateral error. The error should increase with speed since we get fewer samples per decimetre. This cannot be seen here and is probably hidden in other larger errors.

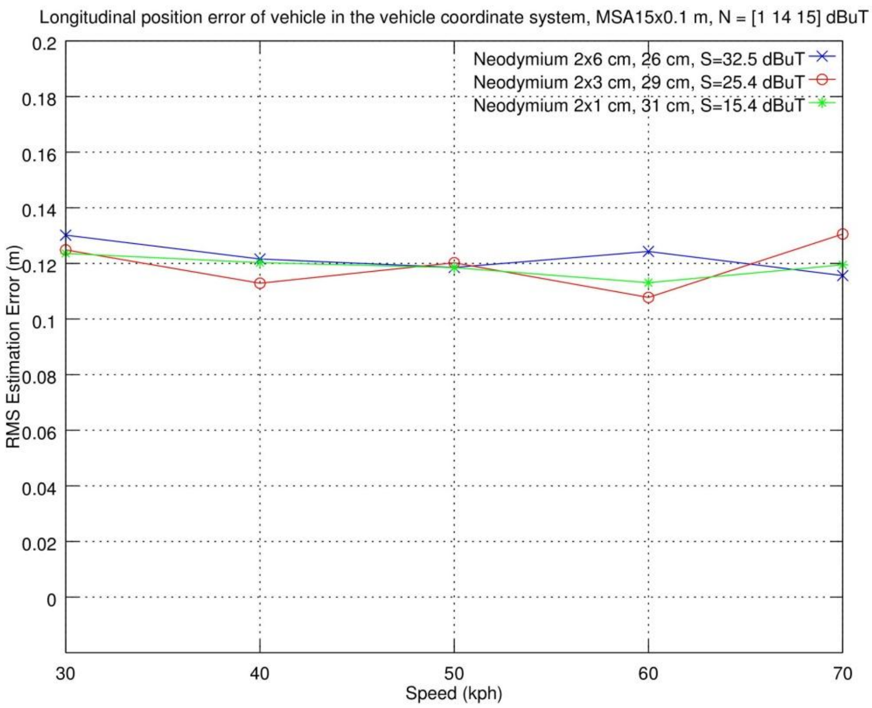

Figure 29 RMS error of the position estimate in the vehicle's longitudinal direction, x, using recorded forest road magnetic sensor data for 15 sensors 10 cm apart with noise = 1, 14, 15 dBµT for AU1, AU2, and AU3

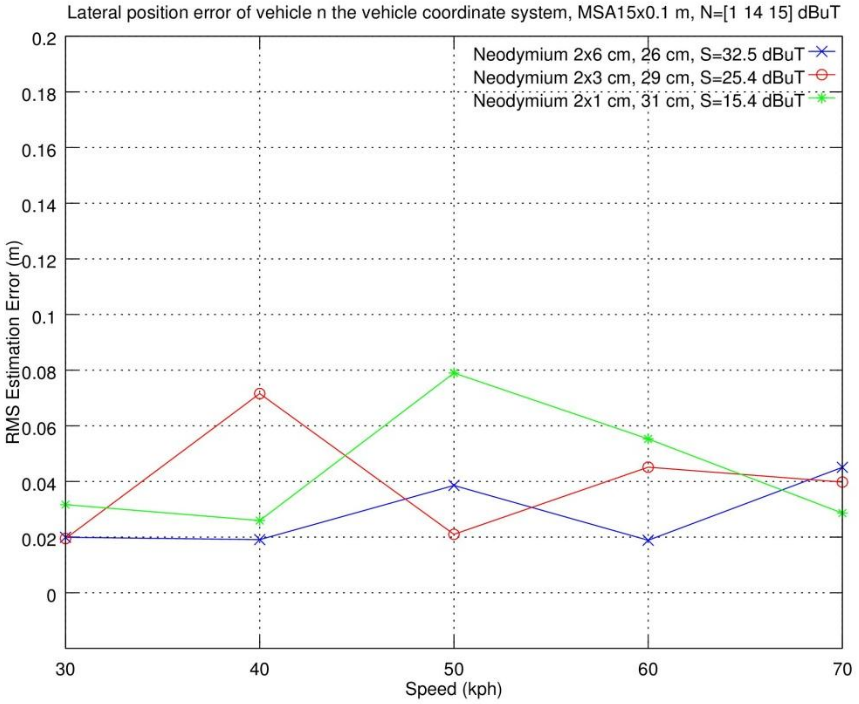

Figure 30 RMS error of the position estimate in the vehicle's lateral direction, y, using recorded forest road magnetic sensor data for 15 sensors 10 cm apart with noise = 1, 14, 15 dBµT for AU1, AU2, and AU3

6.1.6 Difference between simulated and measured

All error graphs presented above are the RMS error of the longitudinal and lateral estimation error in the vehicle's coordinate system. RMS errors from measurements are presented in Figure 30 and Figure 31. Figure 23 and Figure 24 shows the corresponding curves from simulation. The presented RMS errors from measurements are much larger. This is due to three key factors:

1. To estimate the RMS error of the algorithm, the true GPS position and the true heading of the vehicle are needed. Both are unavailable in measured data and are estimated using the vehicle's RT-3002 GPS. The positioning error of this GPS is 5 to 10 cm, which will increase the presented RMS error.
2. Modelling simplifications of the tracking algorithm
3. The simulation environment creates magnetic sensor data that matches all modelling simplifications and provides true GPS position, heading and speed.

The modelling simplifications are based on the following assumptions:

1. The true position and orientation of all markers are known. The forest road markers were measured using the vehicle's RT-3002 system mounted on a carriage that gave a 5 – 10 cm error. The algorithm will then estimate its position with approximately the same error.
2. Vehicle drives on a flat road. The test vehicle moved a lot due to the bumpy forest road. Driving over a bump changes the relative distance between the magnetic sensor array and the ground a lot. Figure 21 shows an amplitude variation in the measurement data.

6.1.7 Results from high speed track data

The key purpose of the high-speed field test was to see if all markers' position and orientation could be found in the vehicle coordinate system at high speed. Thus, the RT-3002 positions of the 50 markers were not measured. In short, the tracking algorithm could detect the distance between the vehicle's origin and the nearest marker with good accuracy in speeds up to 165 km/h. It could also detect the north/south orientation of all 50 markers.

6.1.8 Number of sensors in the sensor array

Based on the results above from simulated data and measured data, it seems to be sufficient to have only 7 sensors 20 cm apart and still fulfil the requirements on maximum lateral and longitudinal RMS error.

6.1.9 Positioning using dead reckoning only

The position can be estimated close to the marker with the accuracy presented in section 6.1.3 to section 6.1.5. Since the distance between the markers are relatively large compared to the decay of the magnetic field it is relevant to understand how the positioning error will increase with distance from a known position.

In this project the positioning error using dead reckoning has not been investigated. The estimate will depend on a number of parameters including the travelled distance. For the analysis in this report Volvo Cars estimate that the lateral and longitudinal dead reckoning RMS error, with sensor configuration of a typical modern vehicle, is smaller than 1.5 cm after a distance of 1 m and smaller than 15 cm after 5 m.

6.1.10 A conservative estimate of the lateral positioning capability

A conservative estimate of the lateral RMS vehicle positioning error is presented in Table 4. The estimate combines the positioning error from the previous sections by adding the uncertainty of the vehicle position close to the marker to the dead reckoning error. The global positioning error should include any uncertainty in the position of the magnetic markers due to e.g. the installation process or any movements in the carriageway over time. The marker positioning error is judged to be less than 2 cm.

Distance from marker (m)	RMS error marker (m)	RMS error dead reckoning (m)	RMS error Combined (m)	Global positioning error (m)
0-0.1	<0.05	NA	<0.05	< 0.07
1	NA	<0.02	<0.07	<0.09
5	NA	<0.15	<0.2	<0.22

Table 4 Estimated RMS lateral positioning error budget.

Thus a global lateral positioning error less than 0.2 meters can be achieved as long as the travelled distance from the marker is less than approximately 3-4 meters.

An implementation of the filtering framework described in section 3.3.3 combines the two estimates and can be expected to give a more accurate estimate.

6.2 Selection of magnetic markers

The intensity of the magnetic marker depends on the volume of the magnet, the material and the distance from the sensor. The data shows that it has to be possible to detect a magnet at a distance of 50 cm. The system would then be used by vehicles that are higher than cars, the system would be less sensitive against variations of asphalt thickness and layers of snow and the marker could be buried at a depth that makes it unaffected by road maintenance, i.e. asphalt milling. The gathered data also shows that it is preferable to have a marker that has a field intensity of at least 8 µT at this height.

Either a neodymium or a ferrite cylinder magnet could be used; they will differ in dimension and cost (the cost is discussed in section 6.8). From an environmental perspective the ferrite magnets is preferable which is an important factor considering a large scale implementation. A ferrite that has an intensity of 8 µT would, according to Figure 48, be 3.0 cm in diameter and 3.5 cm in length. From Figure 45 it can be deduced that the 3×5 cm or 3×6 cm magnets would also be detectable at some distance from the marker.

The origin has so far been located in the centre of the magnet but for the selection of a suitable marker the top of the magnet is a better reference. The distance between the marker's top and the sensor is still set to 50 cm, as the top differs a few centimetres from the centre and the exact distance will vary between vehicles. The optimisation problem then is to find a magnet that has a dimension that gives a field intensity of 8 µT at a height of 50 cm from the top of the magnet but where the volume is as small as possible. The volume is directly correlated to the cost of the marker so there is a clear requirement to keep it small.

The longer the cylinder, the higher the distance between the centre of the magnet and the top of the magnet and hence the field intensity needs to be higher to reach 8 µT at the selected height. A study was performed where all ferrite magnets that fulfilled the requirements where plotted and the magnet with the smallest volume was identified. The ferrite magnet with the least volume is a 4×1.5 cm with a volume of 18.85 cm^3, see Figure 31. The corresponding neodymium magnet would be 2.9×1 cm with a volume of 6.61 cm^3.

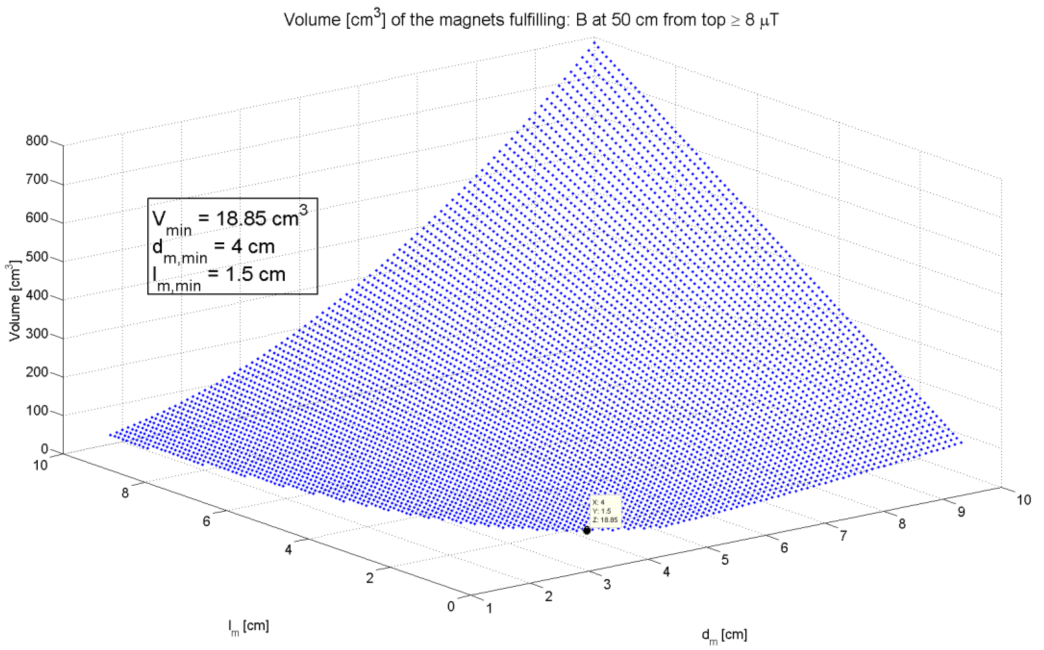

Figure 31 All ferrite magnets that have a field intensity of at least 8 µT at 50 cm from the top of the magnet

6.2.1 Other geometries than cylinders

Through this report a cylindrical magnet is proposed as the other two classical forms for magnets, a cuboid and a ring, both have weaker magnetic field at the required distances. The question then is if there are any other geometries or arrangements of magnets to have a stronger magnetic field with the same or preferably smaller magnet? Two suggestions have been investigated. The first one is to use a parabolic reflector beneath the cylinder to focus the magnetic field and get a higher intensity at a selected height. The short answer is that magnetic fields don't work that way and it won't work, it will even weaken the field for this purpose.

The other suggestion is to use two cylinder magnets connected with a metal rod to create a horseshoe like magnet. An extensive study was not performed as it is a complex problem with many different parameters to model but one model was developed and studied. Two cylinder magnets was placed parallel to each other with a surface-to-surface distance of 1 cm. The magnets was connected for practical reasons with a U-shaped iron rod (μ_r=5000) instead of a straight rod and the dimensions for the magnets was sought that would create a magnetic field intensity of at least 8 µT at a height of 50 cm from the top of the magnets. The result is presented in Figure 32.

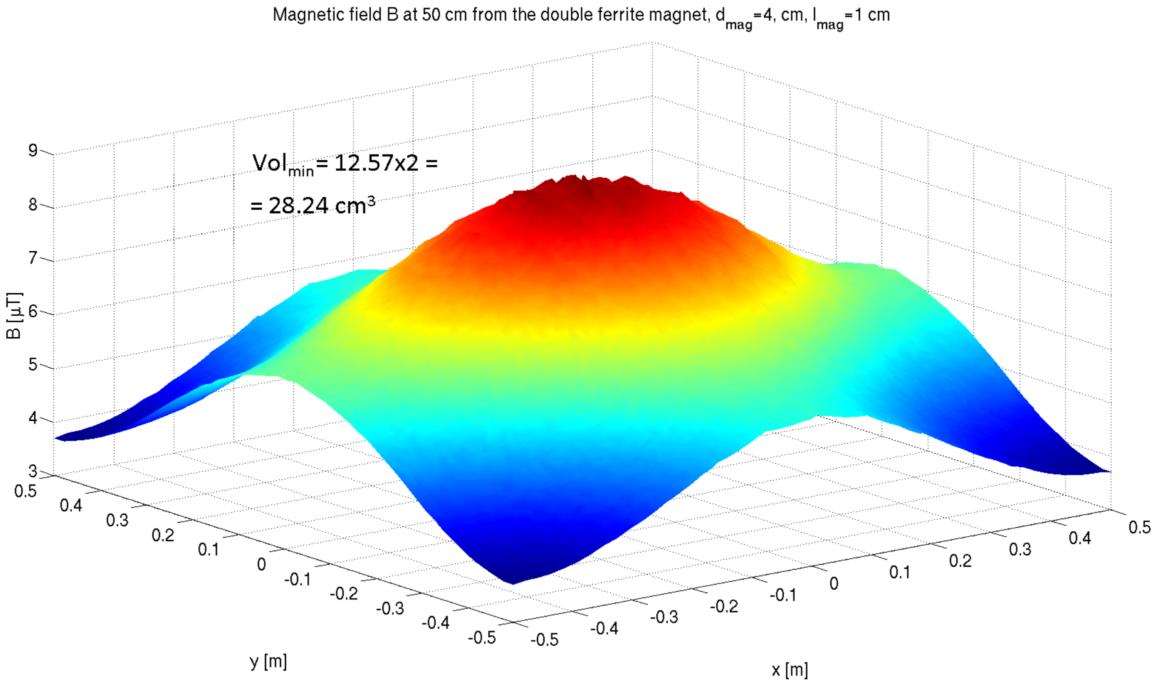

Figure 32 Magnetic field intensity from a dual magnet in a horseshoe shaped configuration

The conclusion that can be drawn from this study is that the magnetic field is wider and the volume of the necessary magnet is nearly doubled. A 4×1.5 cm cylinder has a volume of 18.8 cm^3 which should be compared with the 28.2 cm^3 needed for the horseshoe shaped dual magnet; it is an increase with 49 %.

6.3 Magnetic Pattern

The pattern of the markers in the carriageway is crucial for the overall performance and cost of the system. The application, i.e. what the system is used for, is just one of many parameters that influence the recommendation of a pattern.

6.3.1 Viability of encoding information in the marker pattern

A common proposal when a magnetic marker system is discussed is the usage of the marker's magnetic orientation to encode a bit pattern (e.g. north upwards encodes a binary one and south upwards encodes a binary zero) to send messages to the vehicle [1]. But encoding information like the road geometry might not be flexible enough, consider for example when a new road is constructed. If the vehicle shall depend on the information in the road, then that information has to be tamperproof and have information that "never" needs to be changed – or it has to be easy to "edit" the information. All of these scenarios will increase the cost of maintenance and construction of the marker system.

Modern cars, and especially cars of the future, are commonly connected to a communication network like the mobile phone network. Information about the road's geometry ahead and temporary deviation like road construction sites can much more easily be automatically downloaded from the internet then inserted into the road.

Reference numbers could be encoded in the magnetic pattern. For example the number *137* could encode for "E6, Lackarebäck-Kallebäck, middle lane, northbound" and could be found in a cloud-based database. The feature is not further elaborated in this report as this needs further studying.

6.3.2 Pattern of magnetic markers

The pattern to which the markers are inserted in the carriageway is nearly as important as the intensity of the magnets to be able to detect and predict the vehicle's position. This pattern can be very simplistic, with just one line of markers in the middle of the lane, or it can be very complicated, nearly resembling a matrix barcode [17] in complexity. The more complex the pattern, the more computing power is needed by the system to be able to hold the measured data and interpret the pattern – and it will increase the cost of the system as more markers will be needed. In the analysis below we have chosen to focus on finding a simple pattern that fulfils the requirements and where the constraints are easy to understand.

Two of the requirements were to propose a cost per road meter and that a vehicle that has at a least one set of wheels on the carriageway road is able to detect the markers and estimate the ego position. The latter means that the vehicle in worst case will be mostly off road and only have the left side wheels on the hard shoulder of the road.

In the following discussion it is assumed that the sensors are located so that the sensor will be able to detect a marker up to 30 cm to the side of the vehicle, if this is the case or not depends on the depth of the marker, the height of the vehicle and the placement of the sensors. Those parameters for this discussion are assumed to amount to a detection range (S_{SR} for Sensor Side Range) of 30 cm to the sides of the vehicle. This is a conservative assumption considering the finding above but considered to be reasonable.

6.3.2.1 Pattern analysis, lateral direction

An overview of the situation is shown in Figure 33 where R_S is the width of the hard shoulder and R_L is the lane width. A two lane, one in each direction, carriageway is assumed in this example but the discussion is analogue for wider roads. The lane width (R_L) is assumed to be 3.25 m as this is a common width for Swedish roads [18] and as many roads, as the one shown in Figure 33, are 8 m wide this gives that the shoulder width (R_S) is 0.75 m [19]. These dimensions vary between roads depending on when they were built, a road built to VR 80 standard is assumed (see [18] and [19]).

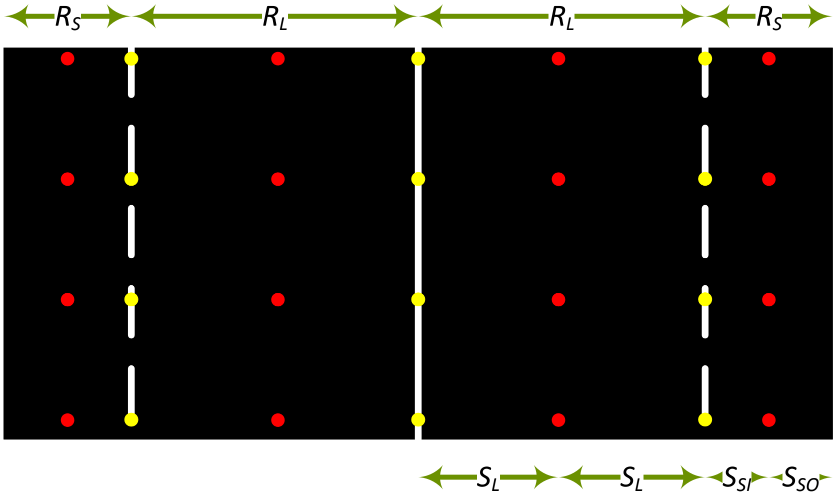

Figure 33 An overview of the carriageway and the proposed marker pattern shown in red and yellow

The width of the vehicle, as defined as the distance between the outer side of the wheels, is denoted as V_W and as the detection range of the sensors in the vehicle's lateral direction is the width of the vehicle plus two times the senor's lateral range; $V_L = V_W + 2 \times S_{SR}$. The track width of a Volvo S60 is 1.6 meters, which gives a V_L of 2.2 meters. This means that if two rows of markers are closer to each other than 2.2 meters, then the sensors will detect both of them. This distance will be crucial to the discussion below.

The distance from the side of the hard shoulder to the marker line on the shoulder, Sensor Shoulder Outer (S_{SO}), is defined by the worst case placement of a vehicle. As it is a requirement that at least one set of wheels should be placed on the hard shoulder, then it will be assumed for the following discussion that S_{SO} is 50 cm (30 cm plus 20 cm for the wheel). The width of the shoulder varies between roads so the Sensor Shoulder Inner (S_{SI}) distance will vary accordingly. As a VR 80 road is assumed S_{SI} is 0.25 m.

The row of markers in the lane is positioned in the middle of it and as R_L is 3.25 m, S_L is 1.63 m. The distance between the lane markers and the shoulder markers is for this road $\frac{S_L}{2} + S_{SI}$ or 1.88 m. When the example vehicle drives in the middle of the lane it will detect the lane's markers but not the shoulder's markers as half of V_L is 1.1 meter, which is less than 1.88 m.

As long as the vehicle is driving in the lane it will be above the markers, as S_L is less than V_L. If the vehicle loses the markers, then it has departed the lane to the right and the tracking system will have noted this. If it departs to the right it would have already detected the shoulder markers long before it loses the mid-lane markers, unless the shoulder is very wide. If the vehicle departs to the right then it will lose all markers and it is possible to drive indefinitely without any markers identified.

The crucial conditions are the two scenarios where the shoulder is so wide that a vehicle can pass between the marker lines and when a vehicle is between the lane markers. To prevent this situation a new set of markers could be introduced, the yellow markers in Figure 33, but if such an approach is advisable depends on the application of the system. It is suggested that these markers are placed in a different pattern from the markers used for normal positioning as these are used for safety – it can be quite dangerous to cross into the next lane or swivel into the shoulder.

The orientation of the magnets is alternated (North, South, North …) for the lane and shoulder markers and only south markers for the markers between the lanes and only north markers for the markers between the lane and the shoulder. This would of course prevent any possibility to use the orientation of the magnets to convey a message to the vehicle.

One problem that needs to be handled is the calibration of the system, at some intervals a calibration track might need to be included. This is not necessary for the magnetic detection system but for the positioning algorithm to verify the calculated position and get a position with a very low error rate. These calibration tracks might be very simple or more complex, all according to the application, but in this proposal it is assumed that such a track is not needed.

6.3.2.2 Pattern analysis, longitudinal direction

The case for the density of the pattern in the longitudinal direction, i.e. along the road, depends on the turning circle of the vehicle as it is shouldn't be possible to do slalom between magnets. As the lateral distance is smaller than the width of the vehicle it won't be possible to move between lateral lines of magnetic markers. It has already been established that the maximum distance that inertial sensor's error is within acceptable bounds is three meters, so the following model can be used.

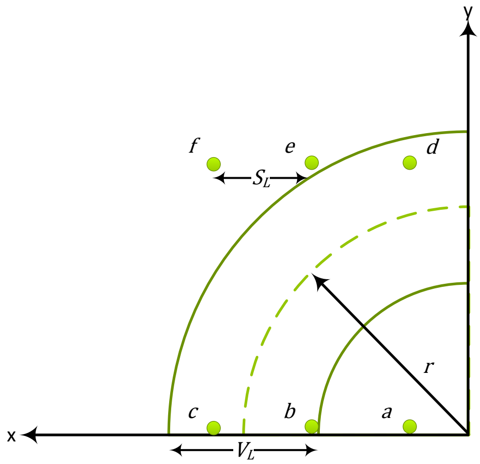

Figure 34 Worst case movement of vehicle, figure is not to scale

The lines in Figure 34 represent the movement of a vehicle and the circles marked *a*-*f* is the markers. The dashed line is the centre of the car and the solid lines the area where markers are detected. Worst case scenario is when the marker *b* is at the right hand side of the detection area. The turning circle, D_{TC}, of a Volvo S60 is 11.3 m which gives a $r = \frac{D_{TC}}{2} = 5.65$ meters. The question then is what position the marker *e* has to be on along the *y*-axis for the sensors to miss it. The length, *l*, along the dashed line from the *x*-axis should not be longer than three meters.

$$m_{e,y} = \frac{D_{TC}}{2} \sin\frac{l}{r} = \frac{11.3}{2} \sin\frac{3.0}{5.65} \approx 2.86\ [m]$$

Equation 8 Calculating maximum distance between markers in longitudinal direction

The proposal then is to have the markers on a distance of 2.8 meters, in that case the marker *e* won't be missed and the position is once again established with high accuracy.

The practical turning circle for a vehicle moving in e.g. 70 km/h is larger and hence a longer distance between the markers is possible at that speed. Thus, for a given spectra of applications it is possible to find a pattern with less markers per area unit. But the result presented above give a hint of the expected cost in a worst case scenario.

6.4 Reliability

A safety-related system is useless without a high reliability, and the reliability of the in-vehicle system can be considered to be high. There is no evidence that it will have significantly lower reliability then similar systems in the vehicle.

The marker system's reliability will depend on a few different circumstances. The magnetic properties in the material of the carriageway will affect the magnetic field and this noise will, from the point of the vehicle, be random in nature. As there doesn't exist any records about what kind of material has been used to construct the road, apart from "cheap stone from the nearby area" [6], it is not possible to draw conclusions. The noise due to the road will be one of many components in the total noise recorded by the system.

Other sources of noise that can affect the system are the local rock deposits, which also will affect local variation of Earth's magnetic field. This will add to the noise but won't fluctuate so much over a distance that it will severely interfere with the system, i.e. make the system make false detections of markers or miss markers. The other side of the interference is noise and that will become a problem if the signal-to-noise ratio becomes so bad that the signal is lost. The system can be designed with this in mind and modern algorithms are very good to find a known pattern in a very noisy signal.

Earth's magnetic field is defined by SGU as being 51 µT [20] but that is mostly in the same plane as the road, the field along the z-axis is very small and as the system measures the magnet's orientation purely in the z-axis the noise from Earth's magnetic field is negligible.

There exist very few other potential natural source of interference; as long as the object has no magnetic properties all magnetic fields will consider it to be air. If it does contain magnetic impurities, then it will interfere but in most cases just add to the general, static noise. The object won't affect the magnets themselves.

Nature has few means to interfere with the system, but human made objects have a higher chance to interfere. Any electric cable that contains an alternating current, that is all of them, will induce a magnetic field which might interfere with the system.

All of these add a component to the noise detected by the system and most of them can be measured and handled during planning of a "magnetic road" and during construction. Apart from actual removal of magnetic sources, there is a possibility to use stronger markers on specifically noisy roads.

The one cause that can make the magnet to alter its field is temperature. As the magnetic field depends on the temperature, see section 3.2.1, this will add to the recorded noise. Considering that the highest temperature recorded in Sweden is 38°C and the lowest is -52.6°C [21] and that the temperature of the road follows the ambient temperature (see section 3.3.1), then the magnetic field will change according to Table 5.

Magnet	Field at -52°C	Field at +38°C
Neodymium	+7,9	-2 %
Ferrite	+13,7%	-3,4 %

Table 5 Decrease of magnetic field at extreme temperatures

The temperature of the marker inserted at some depth in the carriageway will depend on a number of parameters, see section 3.4.

Other environmental effects that can interfere with the system have not been identified apart from that heavy snowfall can increase the distance between the sensor and the marker. This is included when a recommended distance is used in the calculations in this report.

6.5 Fault tolerance

Any system is vulnerable to tampering, intentional or accidental, and systems where anyone can access the system are the most vulnerable. It won't be possible to keep the pattern secret, so any pattern needs to be tamperproof and the detection system tolerant for missed or rough markers. It is very easy to add rough magnets and it is not feasible to try to measure the intensity of the markers and estimate if these are valid or not. The intensity of the magnetic field is used to determine distance and direction to the magnet and trying to validate something that is used for measurement in the same measurement is not deemed to be practical, without added cost to the in-vehicle system.

The current algorithm will detect a faulty marker, either the lack of one or an unexpected one, and will change its current state and search for a new tracking state. The error handling is not currently implemented but as the algorithm detects the situation, a new error handling state can be introduced.

A lot of research has gone into fault tolerance for data communication and signal processing and an extensive literature study has not been performed for this report. Magnetic positioning has several issues in common with radar detection or data communication and it is possible to draw conclusions from those areas. By placing the magnets with high accuracy, using other systems in the vehicle like the GPS and inertial sensors and using a fault correcting pattern, a faulty marker can be detected.

6.6 Maintenance

One of the requirements is that the in-vehicle and the roadside system both shall be maintenance free. There is no indication that the in-vehicle system should require anything else then the general maintenance cycles and requirements of similar sensor systems in the vehicle.

The magnetic marker system might require some maintenance due to the reasons outlined in this report. The magnet is assumed to be encased in a plastic container that protects the magnets from the chemical environment, i.e. from rust, and from the mechanical handling when assembling the pattern. The lifetime of the container will dictate how long it takes before the magnet starts to rust.

Any assembling of the markers has to take the temperature properties, see 3.2.1, of the magnets into account, e.g. hot asphalt should not be poured over the marker without control of the temperature.

6.7 Estimated cost of a system ready for production

The viability of a magnetic detection system depends very much on the price of the in- vehicle system – a high price won't lead to a high adaption. The prototype that has been described in this report is quite far from a system ready for production, but based on the following assumptions a price can be calculated:

1. A production volume of 50,000, all units assumed equal, the system will not be adapted to different models or types of vehicles.
2. The system is only a smart sensor – the system only reports a position over a CAN bus without any integration with other systems in the vehicle, i.e. any indication to the driver is implemented in other systems.
3. The position reported is the lateral position relative to the markers in the current lane (if the vehicle departs from the lane the new position will be relative to the markers in the new lane, there is no knowledge of which lane the vehicle is in). The longitudinal position reported is the distance travelled along the lane, calculated using magnets passed and the inertial sensors etc. available in the vehicle.
4. The system consists of several units with cables in-between.
5. There is a need for seven evenly spaced HMC1022 sensors.
6. The microcontroller is sufficient; the microcontroller used in another smart sensor of similar concept is in the same price range.

Part	Estimated cost
HMC1022	SEK 210
Plastic and cabling	SEK 205
Manufacturing	SEK 115
Microcontroller	SEK 100
Memory	SEK 25
PCB and additional minor components	SEK 135
Sum:	SEK 690

Table 6 Estimated cost of one system

The estimated cost reported in Table 6 above is based on list prices and experience points to that this could be halved when the product is industrialised. Hence the cost of the in-vehicle system is expected to be well below the required cost of SEK 500 at 50,000 units.

6.8 Estimated cost of marker system

The proposal according to the reasoning in section 6.2.1 above is to have a marker pattern (as shown in red and yellow in Figure 33) that is a line of markers in the middle of each lane, one along each lane boundary and one line on the hard shoulder. The distance between the markers in the longitudinal direction will be 2.8 m.

If a ferrite magnet is selected, each marker would be a 4×1.5 cm magnet, according to section 6.1.8, encased in a plastic container according to section 6.6, which gives an estimated cost of SEK 12.30 per marker. For comparison a corresponding neodymium magnet would be 2.9×1 cm and would cost about SEK 42. The conclusion is to use the 4×1.5 cm ferrite as that one is so very much cheaper and also because of the smaller environmental impact. The mining for neodymium has a severe environmental impact, which is an impact that the ferrite magnets does not have.

A neodymium magnet is an alloy of $Nd_2Fe_{14}B$, usually sintered, where Neodymium is a so called rare earth element and most of it is mined in China with some severe environmental impacts. An unbiased source of information about the mining and environmental effects is hard to come by, most of the reports are part of an ongoing debate and few sources are named. The main source of information is news articles as China keeps all information secret [22].

Neodymium is very common in the Earth's crust but never found as concentrated ores, it is usually found scattered in deposits of other minerals. A ferrite magnet on the other hand is a ceramic material with Fe_2O_3 as the main material. There is number of various compounds that can make up the ferrite material depending on the wanted characteristics and the environmental impact depends on the selected materials, but the mining does not have the same environmental impact as neodymium has.

The cost of the pattern, assuming the configuration shown in Figure 33 above, would be seven markers per 2.8 meter carriageway. To attempt to give an estimation of the cost of insert markers into the carriageway this system was compared with other existing systems for machine assembling of roadside devices. The Swedish Transportation Administration has indicated [6] that it is reasonable to assume for this application a machine cost of SEK 2000 per hour and an assembling speed of 20-40 markers per hour. This would give an estimated assembling cost of SEK 50-100 per marker.

With the assumptions in this section the total would cost would be SEK 155,700 per kilometre.

For comparison, the PATH project [1] calculated a cost of USD 1 for the markers and an assembling cost of 5-10 USD per marker for a manual process. The cost of the PATH project's magnet (a 2.5×10 cm ferrite) cannot be used for comparison as the cost of the material fluctuates on the world market, using the cost model for ferrite material used in this report, the cost of the PATH magnet would be SEK 38. Using the machine estimated assembling of this project but the cost of PATH's magnet at a cost of SEK 6.60 per marker would give a cost of SEK 141,500 per kilometre, using the proposed marker pattern.

7 Conclusions

In this study a sensor system prototype for vehicle positioning by magnets has been designed, implemented and tested. There are many parameters that affect the performance of a positioning system; both in the in-vehicle system, for the magnetic markers and environmental circumstances.

The conclusion is that the road will put some requirements on the marker, but any such requirement is easily handled by selecting a sufficiently strong magnet. By burying the marker at a sufficiently large depth handles the rest of the requirements. Some cases, most notably tunnels and bridges, will require special treatment but that varies on a case by case basis and there isn't any general solution.

The markers need to be selected based on durability, price and field intensity. A high durability should be possible to archive by encasing the magnet in plastic, the durability of the marker will then mostly depend on the durability of the plastic. The field intensity and the price are tightly coupled and a cylindrical ferrite magnet with a diameter of 4.0 cm and a length of 1.5 cm has been found to be optimal to give the desired field intensity at the lowest price. Ferrite magnets have the benefit over the more expensive neodymium magnets that the mining of the materials has lower environmental impact. This is an important issue in a large scale implementation.

The application defines the definite position accuracy for the system, but the measurement performed on the forest road gives that the prototype system had a lateral error of much less than the required 10 cm. The lateral error varied between measurements as the prototype system's design introduced some measurement errors, but the conclusion is that it is possible to design a system with the required accuracy, and even better than that.

A crucial factor that drives the cost of the overall system is the pattern of the markers as the number of markers is directly proportional to the cost of enhancing a road. A minimum of markers would infer a cost of SEK 156 per metre of carriageway. This would require a pattern that consists of seven parallel lines of markers along an ordinary VR 80 road with one lane in each direction and markers will be placed at 2.8 m along these lines.

The pattern is not only determined by the required positioning accuracy, any pattern needs to be tamperproof and fault tolerant. How the pattern is used determines the requirement on to what extent error correction is needed but there is little use of encoding information in the pattern. The conclusion is that since the positions of the markers are known a faulty marker or a marker tampered with can easily be identified and either corrected or ignored. The positioning error might locally increase but as other systems are usually available like GPS and inertial systems the estimate is that the error can be kept within bounds.

What the positioning system is used for determines a lot of parameters but given the constraints outlined in this report an in-vehicle system that would cost about SEK 690 would be possible to design. This system would be a smart sensor, using the information is up to other systems.

The final conclusion is that it is possible, given the constraints and compromises outlined above, to build a system with an estimated cost of SEK 690 for the in-vehicle system and SEK 156 per meter carriageway. As already described experience points to a possibility to meet the requirement of a cost of SEK 500 per unit.

8 Further research and development

Several of the research issues have been resolved in this study as has been outlined in this report, but many more needs further study. The main areas that need further study before a final system can be designed are outlined in the following bullets.

- A set of application scenarios needs to be defined and then the marker pattern and the markers can be optimised. This could mean that different markers and patterns are used for different applications.
- Real-time and on-board vehicle implementation of the system.
- Detailed analysis of a carriageway's movement due to thawing and the temperature gradient of a carriageway around the year.
- Detailed analysis and measurement of the noise level on different roads and also the constraints set by tunnels and bridges.
- Optimising the placement of the sensors in various types of vehicles, depending on application and the vehicle's chassis construction.
- Further analysis of assembling and maintenance of the magnetic markers in regard to different application scenarios.

9 Terminology

AU Acquisition unit.

B_r The remanence field of the magnet, a physical constant. See section 3.2.

B_z The magnetic field intensity along the z-axis at a specific position in space. See section 3.2.

d×l The dimension of a magnet is denoted as the diameter times the length of the magnet. A 3×1 cm magnet has a diameter of 3 cm and a length of 1 cm, see also section 3.1.

μ_0 The permeability of free space. See section 3.2.

μ_r The relative permeability of a material. See section 3.2.

Magnetic orientation The magnet is, unless otherwise specified, a cylindrical magnet and the magnetisation is in the axis of the length of the cylinder. The orientation of the magnet is said to be in the direction which the north pole of the magnet is pointing.

Marker A magnet inserted into the carriageway used for detection; the material, magnetic orientation and size of the magnet is usually undefined.

10 Works Cited

[1] Institute of Transportation Studies, "California PATH," University of California, Berkeley, 2010. [Online]. Available: http://www.path.berkeley.edu/. [Accessed 22 August 2013].

[2] N. Derby and S. Olbert, "Cylindrical magnets and ideal solenoids," *American Journal of Physics,* vol. 78, no. 3, pp. 229-235, 2010.

[3] H. M. Yin and L. Z. Sun, “Magnetic properties of randomly dispersed magnetic particulate composites: A theoretical study,” *Physical Review B,* vol. 72, no. 5, 2005.

[4] Comsol Inc, “COMSOL Multiphysics,” [Online]. Available: http://www.comsol.com/.

[5] Trafikverket, Övergripande krav för vägars och gators utformning, Borlänge: Trafikverket, 2012.

[6] Swedish Transportation Administration, *E-mail correspondences with representatives of Swedish Transportation Administration,* Borlänge, 2013.

[7] Å. Hermansson, “Mathematical Model for Calculation of Pavement Temperatures: Comparison of Calculated and Measured Temperatures,” *Transportation Research Record: Journal of the Transportation Research Board,* vol. Volume 1764 / 2001 Assessing and Evaluating Pavements, pp. 180-188, 2001.

[8] S. F. Said and H. Hakim, “Evaluering av asfaltkonstruktion E6 Fastarp–Heberg,” VTI, Linköping, 2008.

[9] Trafikverket, Trafikverkets tekniska krav Tunnel, Borlänge: Trafikverket, 2011.

[10] Trafikverket, Trafikverkets tekniska krav Bro, Borlänge: Trafikverket, 2011.

[11] J. B. Rawlings, J. G. Ekerdt and J. W. Eaton, “GNU Octave,” Free Software Foundation, 2013. [Online]. Available: http://www.gnu.org/software/octave/. [Accessed September 2013].

[12] Oxford Technical Solutions Limited, “RT3000 Family,” Oxford Technical Solutions Limited, 2013. [Online]. Available: http://www.oxts.com/products/rt3000-family/. [Accessed 29 October 2013].

[13] Honeywell, "1, 2 and 3 Axis Magnetic Sensors HMC1051/HMC1052L/HMC1053," Honeywell, Plymouth, 2010.

[14] STMicroelectronics, “STM32F4DISCOVERY,” STMicroelectronics, 2013. [Online]. Available: http://www.st.com/web/catalog/tools/FM116/SC959/SS1532/PF252419. [Accessed 2013].

[15] D. Meeker, “Finite Element Method Magnetics,” 24 06 2011. [Online]. Available: http://www.femm.info. [Accessed June 2013].

[16] H. G. Xu, C. X. Wang, R. Q. Yang and M. Yang, “Extended Kalman Filter Based Magnetic Guidance for Intelligent Vehicles,” in *Intelligent Vehicles Symposium, 2006 IEEE*, Tokyo, Japan, 2006.

[17] Wikipedia, “Barcode - Wikipedia,” 6 November 2013. [Online]. Available: http://en.wikipedia.org/wiki/Matrix_barcode#Matrix_.282D.29_barcodes. [Accessed 6 November 2013].

[18] Trafikverket, Krav för vägars och gators utformning, Borlänge: Trafikverket, 2012.

[19] Trafikverket, Råd för vägars och gators utformning, Borlänge: Trafikverket, 2012.

[20] Sveriges geologiska undersökning, “Flygmätning - Sveriges geologiska undersökning,” Sveriges geologiska undersökning, [Online]. Available: http://www.sgu.se/sgu/sv/geol_kartering/geofysik/flygmatn_s.htm. [Accessed October 2013].

[21] SMHI, “Väderrekord,” SMHI, 29 September 2012. [Online]. Available: http://www.smhi.se/kunskapsbanken/meteorologi/vaderrekord-1.5782. [Accessed 12 11 2013].

[22] S. Parry and E. Douglas, “In China, the true cost of Britain's clean, green wind power experiment: Pollution on a disastrous scale,” Daily Mail Online, 26 January 2011. [Online]. Available: http://www.dailymail.co.uk/home/moslive/article-1350811/In-China-true-cost-Britains-clean-green-wind-power-experiment-Pollution-disastrous-scale.html. [Accessed 29 November 2013].

11 Appendix

11.1 Magnetic field study

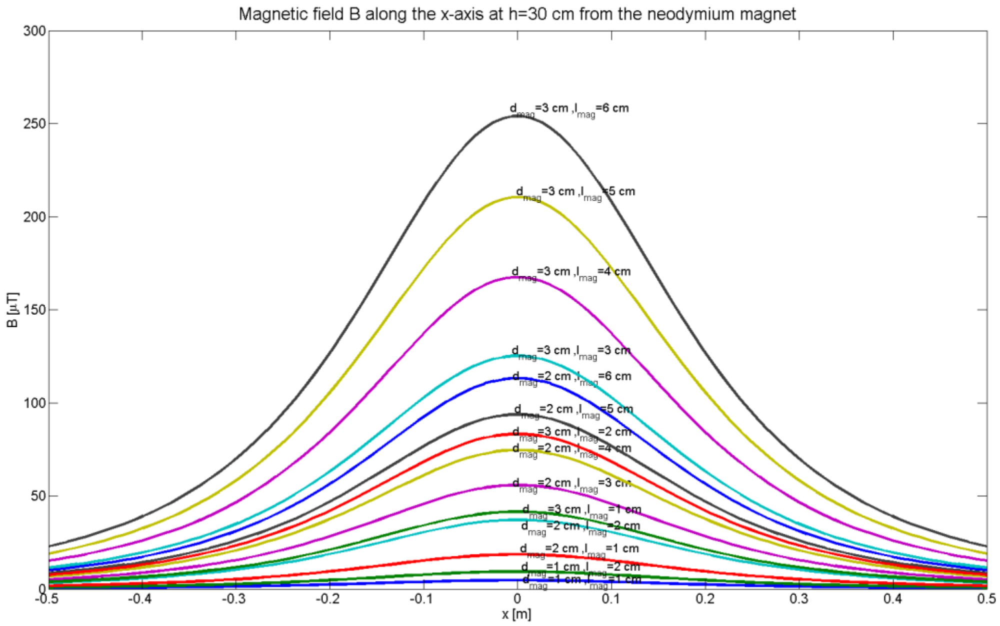

Figure 35 Magnetic field study free space, neodymium, B along x-axis, h=30 cm

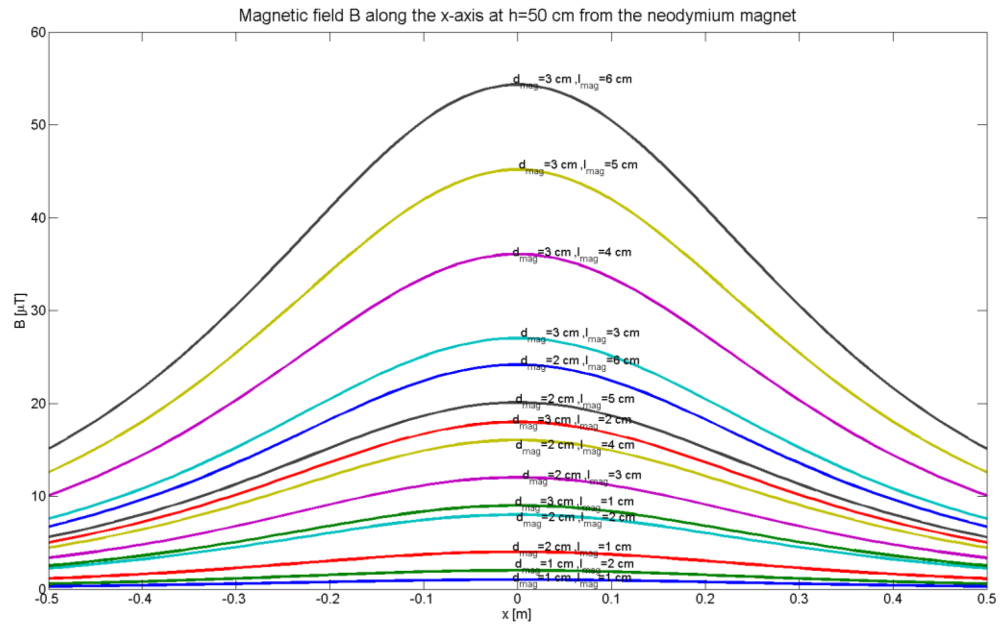

Figure 36 Magnetic field study free space, neodymium, B along x-axis, h=50 cm

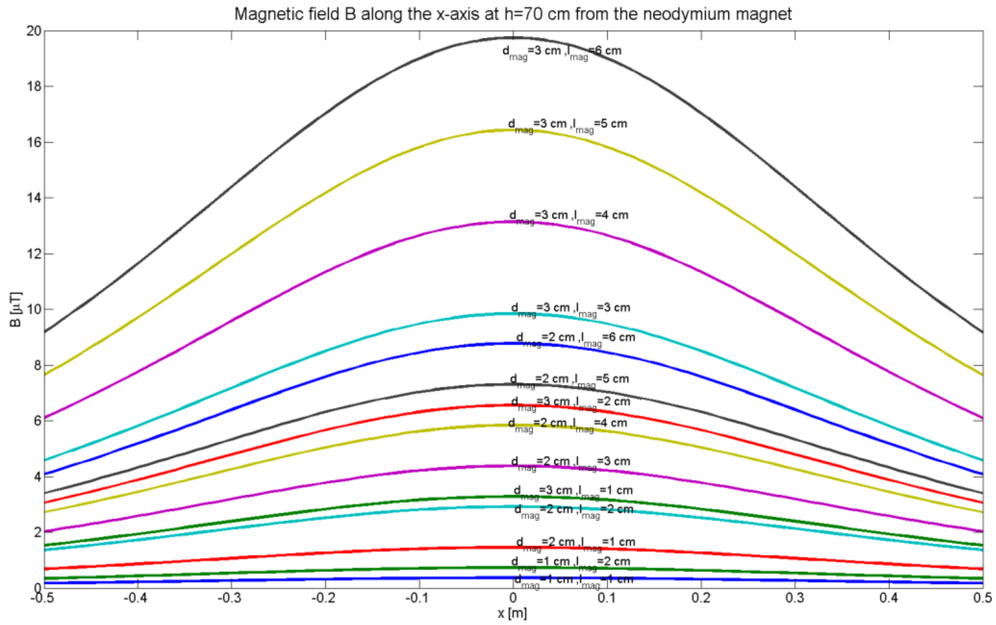

Figure 37 Magnetic field study free space, neodymium, B along x-axis, h=70 cm

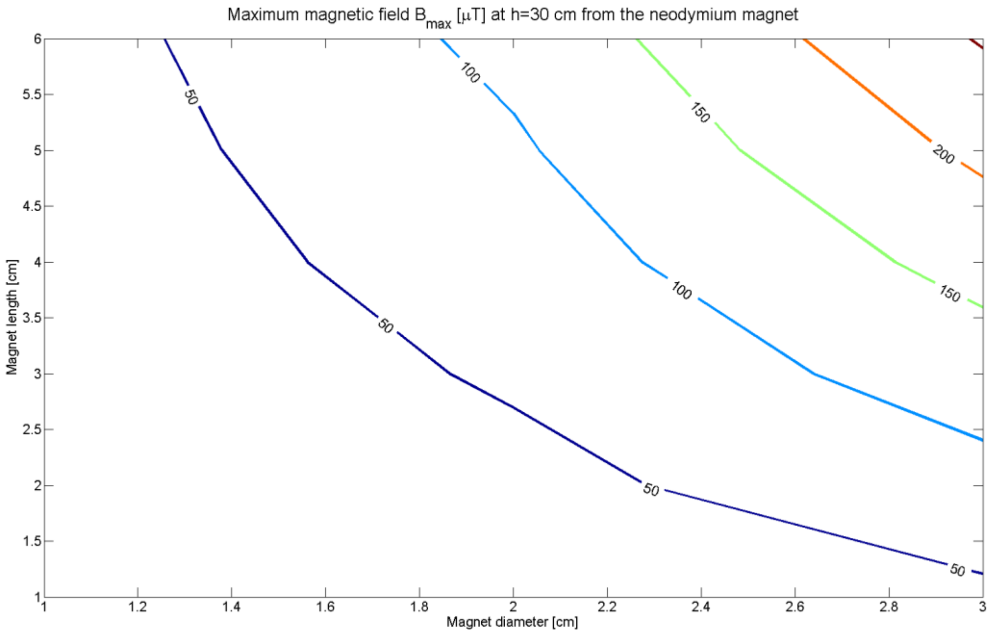

Figure 38 Magnetic field study free space, neodymium, B as function of dimensions, h=30 cm

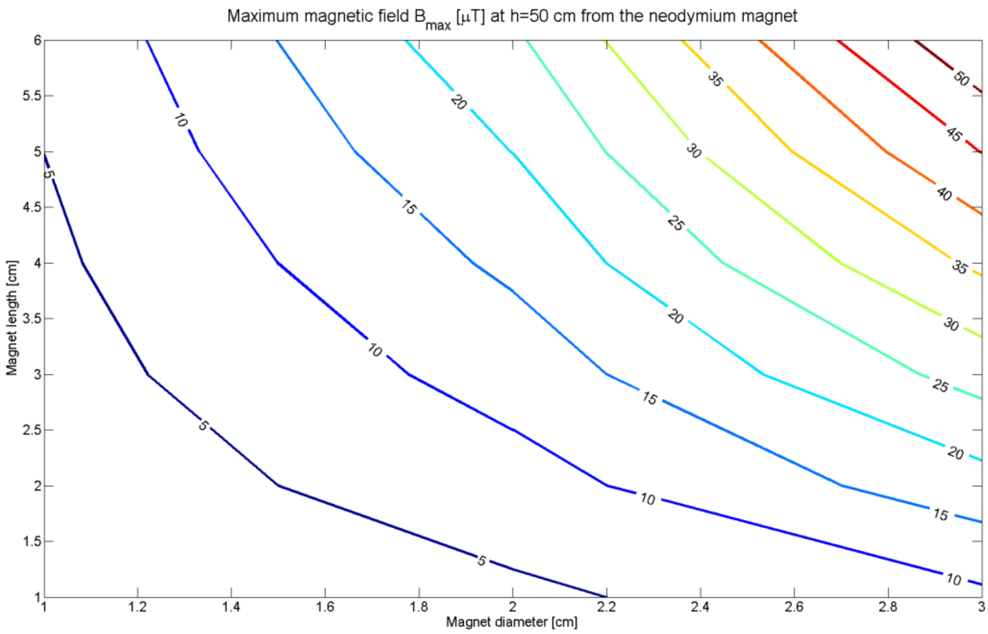

Figure 39 Magnetic field study free space, neodymium, B as function of dimensions, h=50 cm

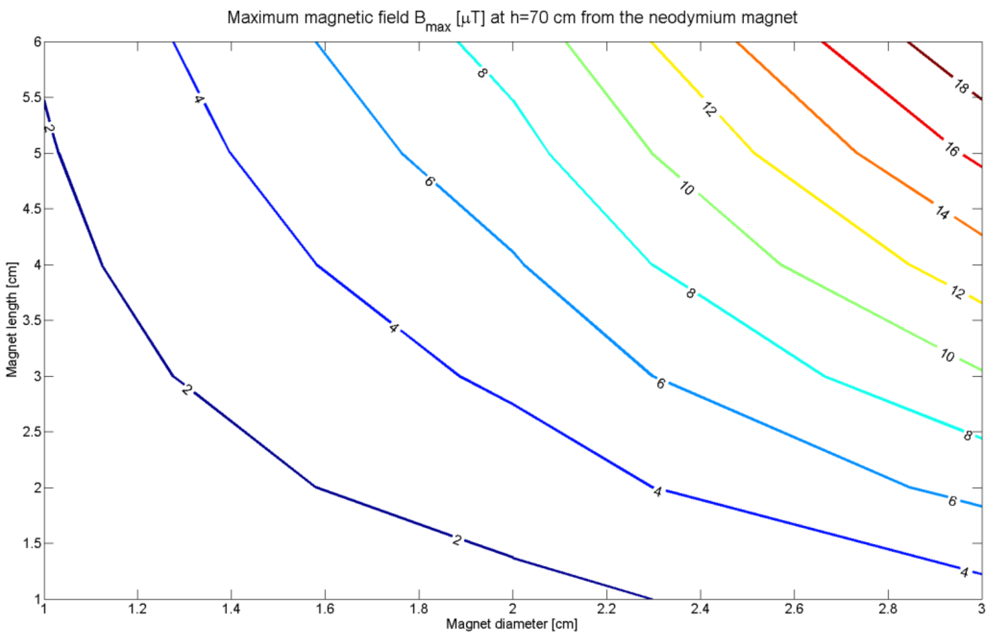

Figure 40 Magnetic field study free space, neodymium, B as function of dimensions, h=70 cm

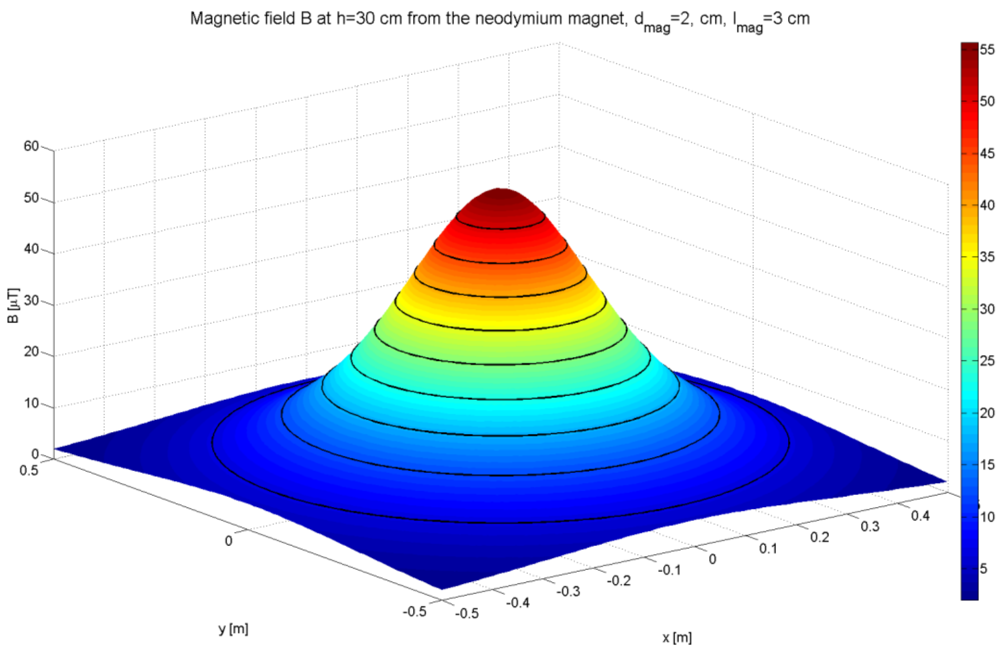

Figure 41 Magnetic field study free space, neodymium, 3D plot of B, h=30 cm

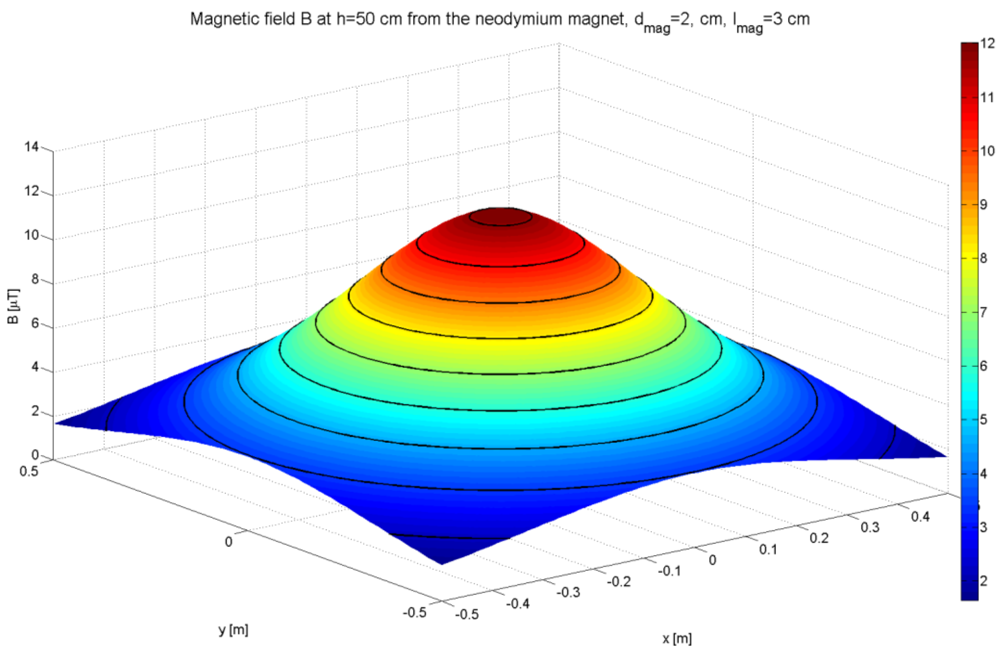

Figure 42 Magnetic field study free space, neodymium, 3D plot of B, h=50 cm

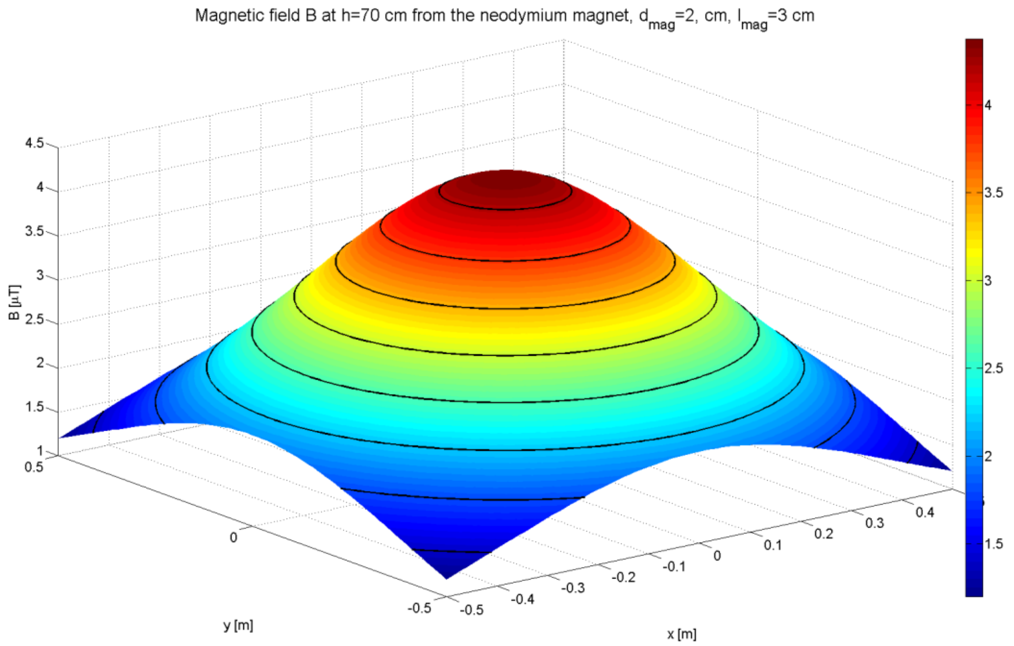

Figure 43 Magnetic field study free space, neodymium, 3D plot of B, h=70 cm

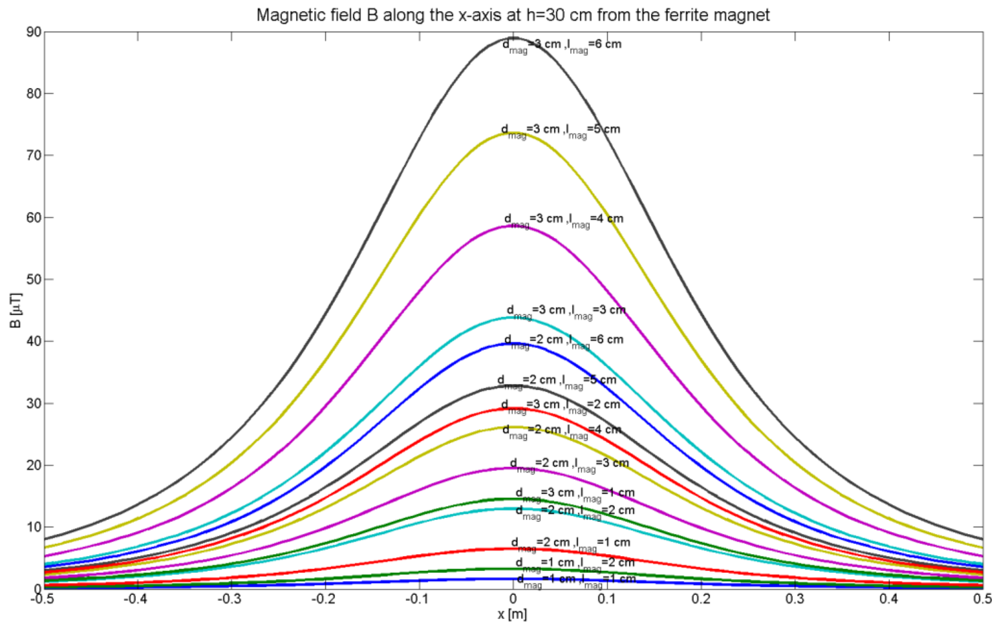

Figure 44 Magnetic field study free space, ferrite, B along x-axis, h=30 cm

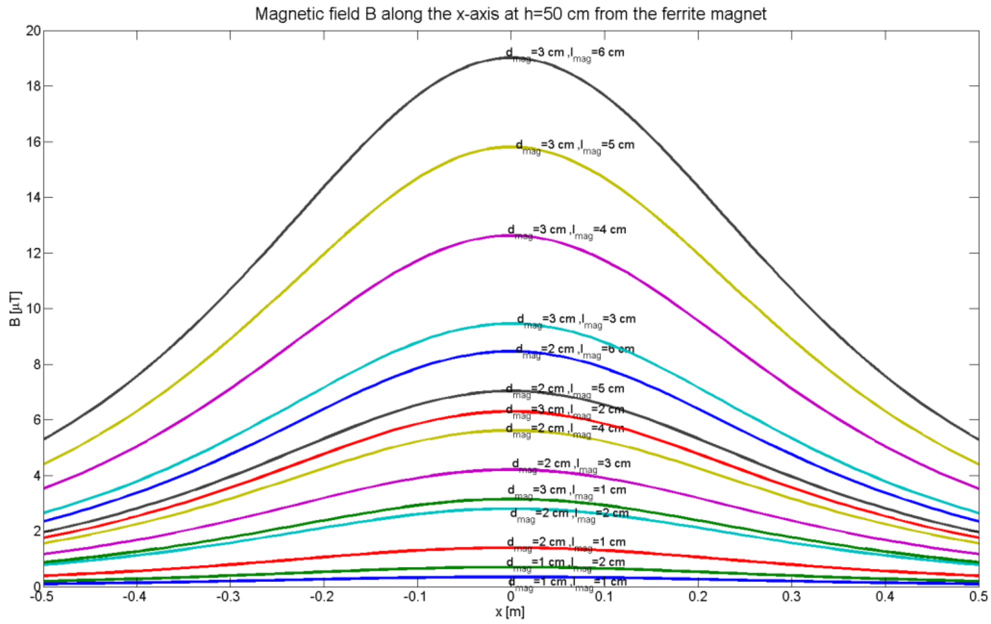

Figure 45 Magnetic field study free space, ferrite, B along x-axis, h=50 cm

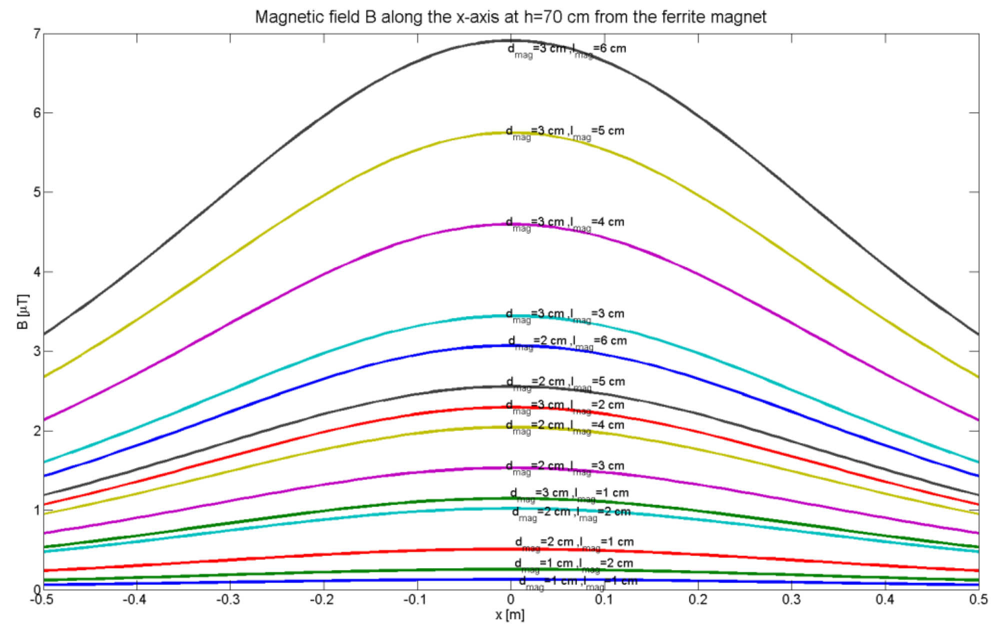

Figure 46 Magnetic field study free space, ferrite, B along x-axis, h=70 cm

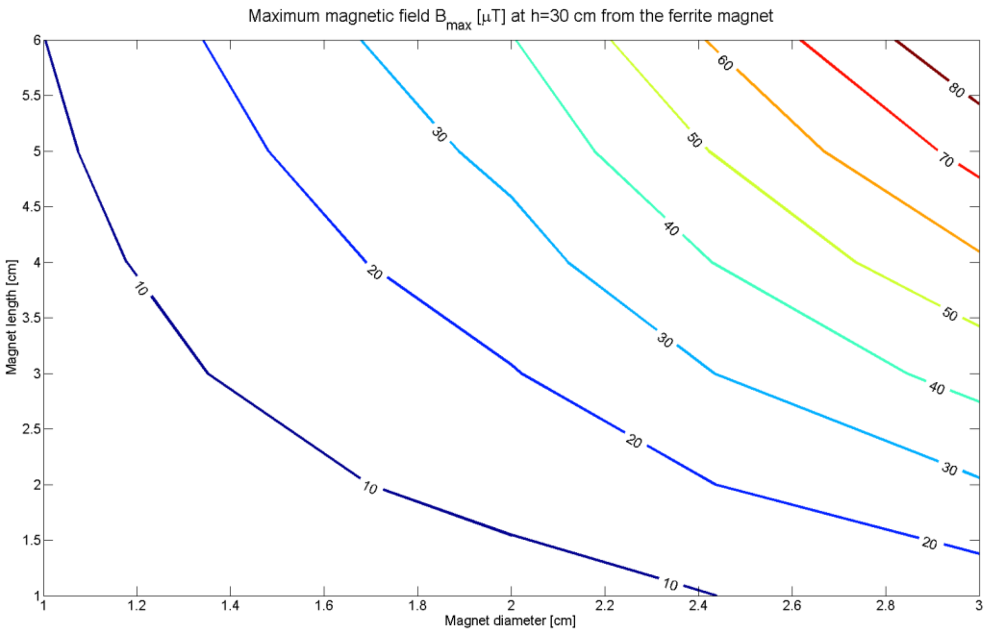

Figure 47 Magnetic field study free space, ferrite, B as function of dimensions, h=30 cm

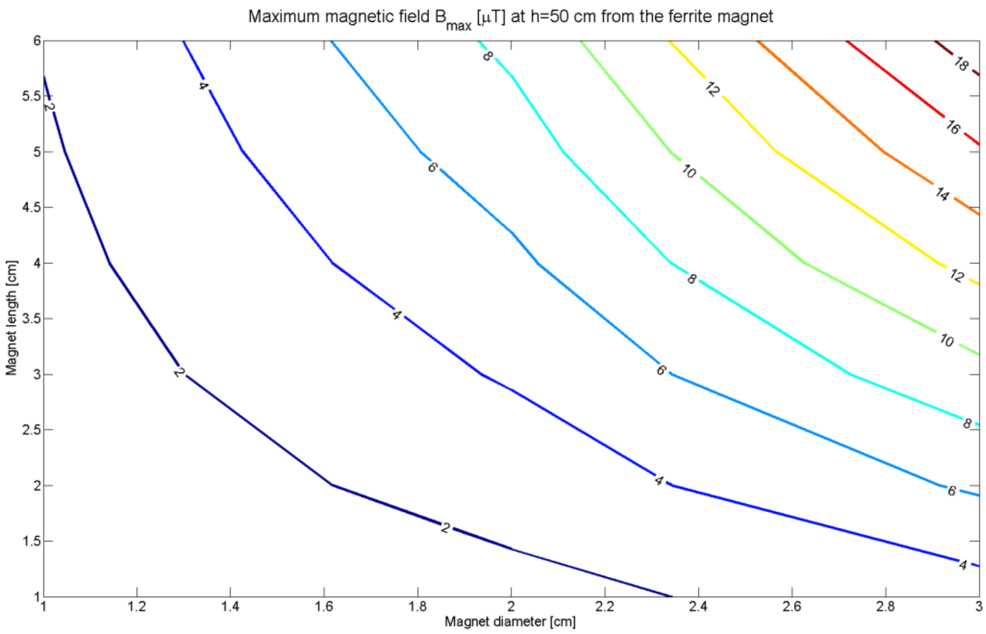

Figure 48 Magnetic field study free space, ferrite, B as function of dimensions, h=50 cm

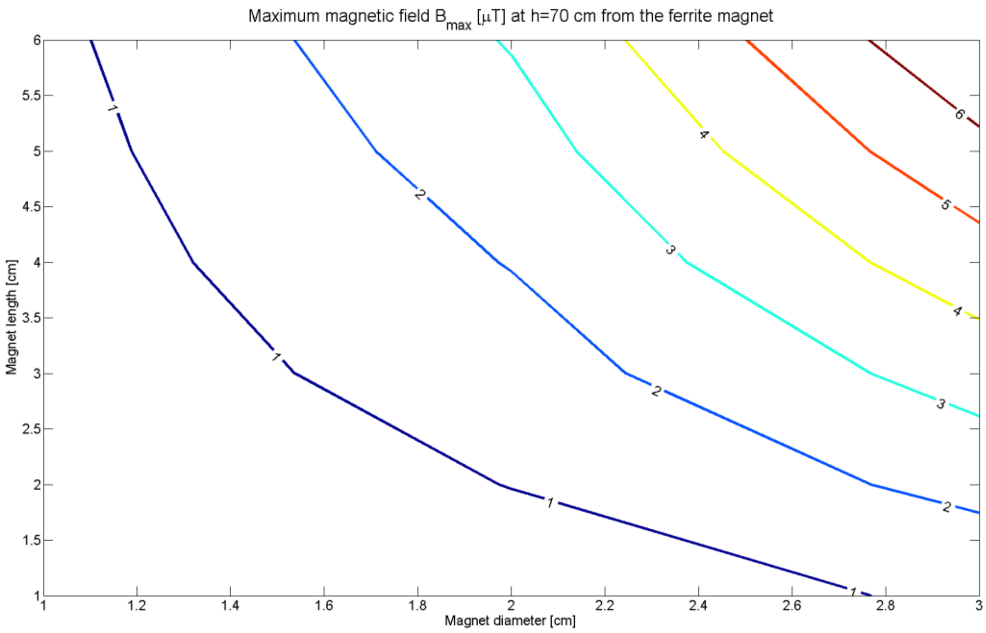

Figure 49 Magnetic field study free space, ferrite, B as function of dimensions, h=70 cm

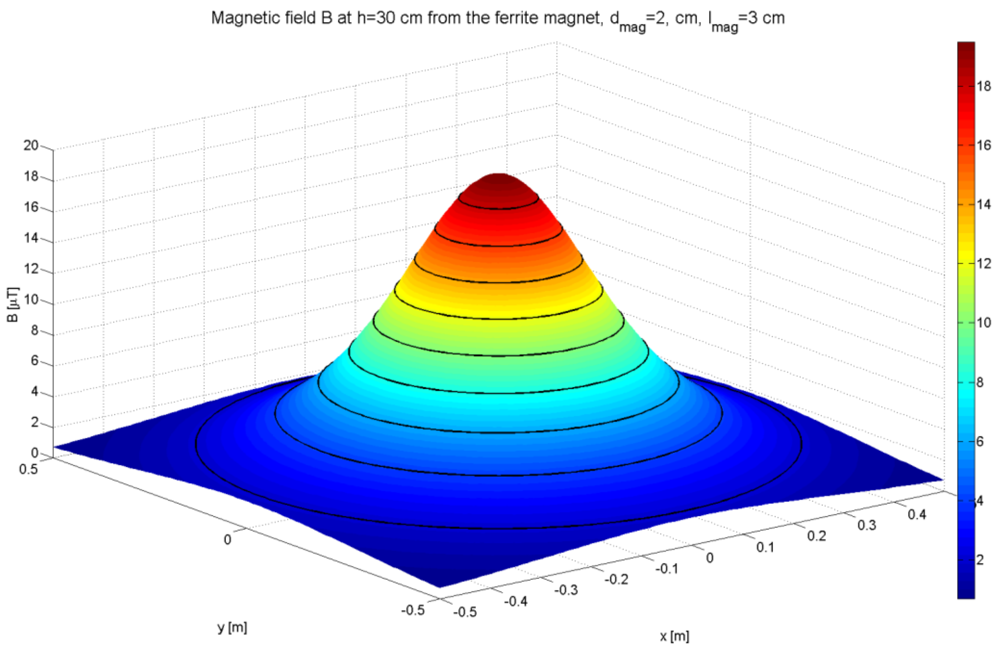

Figure 50 Magnetic field study free space, ferrite, 3D plot of B, h=30 cm

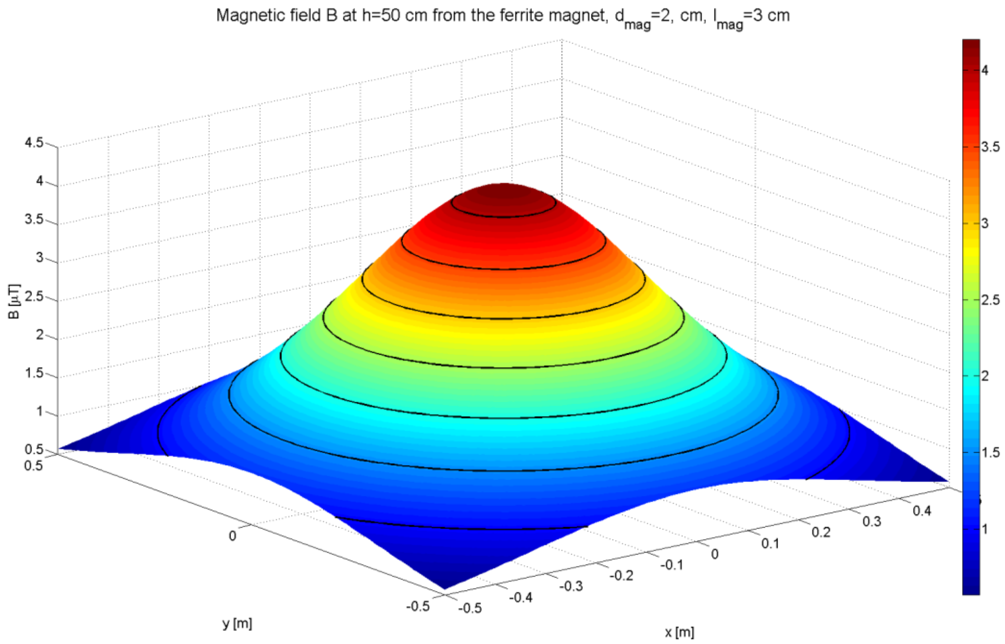

Figure 51 Magnetic field study free space, ferrite, 3D plot of B, h=50 cm

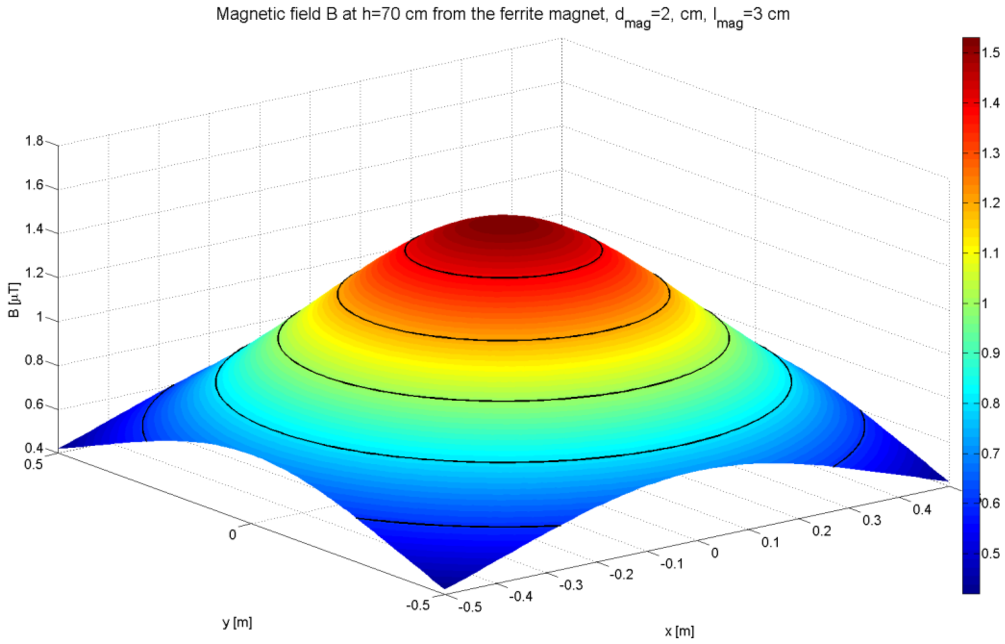

Figure 52 Magnetic field study free space, ferrite, 3D plot of B, h=70 cm